Chemotherapy coupled to macrophage inhibition leads to B cell-mediated T cell memory activation and durable triple negative breast cancer regression

Swarnima Singh[1,2], Nigel Lee[3], Igor Bado[1], Clark Hamor[1], Licheng Zhang[6], Sergio Aguirre[1], JingyuanHu[3], Yichao Shen[1], Yitian Xu[6], Yang Gao[1], Diego Pedroza[1], Na Zhao[1], Shu-Hsia Chen[6], Ying-Wooi Wan[3,8], Zhandong Liu[3,8], Jeffrey T. Chang[4], Daniel Hollern[7], Charles M. Perou[5], Xiang H.F. Zhang[1,2*], Jeffrey M. Rosen[1,2*]

1. Department of Molecular and Cellular Biology and Dan L Duncan Comprehensive Cancer Center, Baylor College of Medicine
2. Translational Biology and Molecular Medicine, Baylor College of Medicine
3. Jan and Dan Duncan Neurological Research Institute at Texas Children's Hospital, Houston, United States
4. Department of Integrative Biology and Pharmacology, The University of Texas Health Science Center at Houston.
5. Lineberger Comprehensive Cancer Center, University of North Carolina, Chapel Hill, NC 27599, USA
6. Immunomonitoring Core, Center for Immunotherapy Research, Houston Methodist Research Institute (HMRI), 6670 Bertner Avenue, R9-330.11, Houston, Texas 77030
7. Salk Institute for Biological Studies, Salk Cancer Center, NOMIS Center for Immunobiology and Microbial Pathogenesis, 10010 N Torrey Pines Rd • La Jolla, CA 92037
8. Department of Molecular and Human Genetics, Baylor College of Medicine

*-Co-corresponding authors

Abstract

Immunosuppressive elements within the tumor microenvironment such as Tumor Associated Macrophages (TAMs) can present a barrier to successful anti-tumor responses by cytolytic T cells. We employed preclinical syngeneic p53 null mouse models of triple negative breast cancer (TNBC) to develop a treatment regimen that harnessed the immunostimulatory effects of low-dose chemotherapy coupled with the pharmacologic inhibition of TAMs. Combination therapy was used to successfully treat several highly aggressive, claudin-low murine mammary tumors and lung metastasis. Using single cell RNA sequencing we uncovered a coordinated interaction between T helper cells and antigen presenting B cells to promote anti-tumor immunity and long-term responses. Using high dimensional imaging techniques, we identified the close spatial localization of B220+ Cd86+ activated B cells with Cd40lg+ Cd4+ T cells in tertiary lymphoid structures that were present up to 6 weeks post treatment. We also characterized the transcriptional and metabolic heterogeneity of tumor associated macrophage populations between closely related tumor models that may impact how they respond to combination treatment. Furthermore, the B cell markers and the signatures derived from the expanded B cells after combination therapy were shown to correlate with the pathologic complete response observed in TNBC patients treated with neoadjuvant chemotherapy. This study illustrates the complexity of the tumor immune microenvironment and highlights different immune responses that result from rationale combinations of immunotherapy.

Introduction

Heterogeneity in TNBC has been well characterized with respect to cancer cell intrinsic (1)features, but much less is known about the contribution of tumor infiltrating immune cells. Immunologically hot tumors that are associated with a better prognosis have a high infiltration of CD8+ T cells; however not all tumors respond equally to checkpoint blockade. Immunosuppressive myeloid cells such as TAMs have been implicated in suppressing anti-tumor T cell responses and promoting angiogenesis (2), tumor invasion, extravasation and metastasis within the dynamic tumor immune microenvironment (TIME) (3) and TNBC patients with a high TAM signature have a poor prognosis (4) .

Our tumor models arose from studies done to evaluate the role of p53 in the development of mammary cancers. Due to the long latency period of mammary tumors and the aggressive nature of p53 deletion induced lymphomas, mammary epithelium from p53 mull mice was transplanted into wildtype Balb/c mice and resulted in the growth of heterogenous mammary adenocarcinomas (5) . Building on this, we developed novel preclinical p53 -/- syngeneic TNBC GEM models including several with a high mutation burden and sensitivity to IO, and others that are highly sensitive to specific chemotherapeutic agents (i.e., CTX or carboplatin) (6) . These unique syngeneic GEM models have been genomically profiled and fall under basal-like, luminal and claudin low tumors, much like human breast tumors (1, 7) . Claudin-low tumors adopt a spindle-like morphology indicative of their highly mesenchymal nature. Recently, they have been characterized with respect to the immune microenvironment and have shown an enrichment in tumor associated macrophages (TAMS) as compared to basal-like tumors (8) . Furthermore, increasing the mutation burden in certain claudin-low tumors has been shown to improve their responsiveness to IO and has been validated in human patient datasets (9) .

Single-cell RNA sequencing as well as profiling of TCR repertoires have proven to be valuable tools to dissect the cellular heterogeneity in various cancers. By combining high dimensional transcriptomic data of individual tumor infiltrating immune cells with bulk RNA sequencing data from the multiple murine mammary tumor models, we have begun to identify the complex dynamics that prevent tumors from undergoing long-term regression in order to uncover additional targets to overcome treatment resistance. Furthermore, we have harnessed the immunostimulatory effects of the low-dose chemotherapeutic agent cyclophosphamide (Cytoxan, CTX) aided by the depletion of immunosuppressive TAMs (Pexidartinib, PXB) to successfully induce durable long-term responses in highly aggressive primary murine mammary tumors. The presence of tertiary lymphoid structures has been associated with responders to checkpoint blockade in melanoma (10) and we observed TLS infiltrated

by CD4+ T helper cells and B220+ Cd86+ B cells in responders to this combination treatment regimen. Activated antigen presenting B cells expressing CD86 and Rel expanded after combination treatment and their signatures correlated with pathological complete responses in patients undergoing neoadjuvant chemotherapy.

Mechanistically, unique ligand receptor interactions between *Traf3* and *CD40lg* mediate class switch recombination in activated B220+ Cd86+B cells leading to a sustained effective anti-tumor immune response at the primary site that persists in TLS long after treatment cessation. We also characterized TAM populations in a phenotypically similar, but recurrent mouse model that may provide useful clues to understand TAM heterogeneity and develop future therapeutics targeting TAM metabolism. We have also shown that combination therapy also can reduce established lung metastasis and show an association with pathologic complete response(pCR) to chemotherapy in TNBC patients. These studies highlight the importance of identifying specific biomarkers to predict patient responses to this treatment combination.

Results

p53 -/- syngeneic TNBC GEM recapitulate human TNBC subtypes and respond to low dose immunostimulatory chemotherapy treatment

A screen using “standard of care” drugs on a claudin-low p53 null syngeneic GEM model of TNBC T11 showed that these tumors were resistant to most conventional chemotherapy treatments but responded to low-dose cyclophosphamide (CTX,100mg/kg) (11) treatment **(Fig S1a).** We utilized another closely related claudin-low model, T12, to understand the basis for this response, in parallel to T11 which has been extensively studied within the context of the tumor immune microenvironment. These tumors have an enrichment for the EMT pathway **(Fig 1a**) and also are highly infiltrated by TAMs **(Fig 1b, Fig S1b)** when compared to other more basal-like or luminal p53 -/- tumor models such as 2225L and 2208L. Principal component analysis also showed that the 3 claudin-low tumor models, namely T12, T11 and 2151R clustered together as compared to tumor models from basal(2225L) and luminal(2208L) subtypes, indicating a certain degree of transcriptomic similarity between these models, however there is still some level of transcriptomic heterogeneity between these 3 models**(Fig 1c)**.This observation lead us to question whether the heterogeneity was related to the immune microenvironment in these tumors, especially in T12 and how this would affect responses to chemotherapy in these claudin-low models

T12 tumors implanted in the mammary fat pads of Balb/c mice and then treated with CTX showed a greater decrease in tumor volume ascompared to T12 CTX treated tumors in NSG mice that lack T Cells, B Cells and functional NK cells **(Fig 1d**), suggesting a possible synergy between T cells and CTX was required for superior T12 tumor cell killing. This was supported by in vitro assays using GFP targeting T Cells derived from JEDI mice (12) that showed a significant increase in cell death of GFP+ T12 cells upon addition of an active metabolite of CTX, phosphoramide mustard (PM), as CTX needs to be metabolized in the liver into its active form and cannot be used in-vitro(13) **(Fig S1e).**

Furthermore, flow cytometry analysis revealed an increase in the numbers of CD4+ and CD8+ T cells in T12 tumors after CTX treatment in immunocompetent Balb/c mice **(Fig S1f).** Antibody depletion of CD4+ resulted in an impaired response to CTX **(Fig 1e)** but did not fully abolish the differences in response between of Balb/c mice compared to NSG mice indicating there could be a cooperative effort between the T cell subtypes as well as other cells NSG mice lack including B cells, that promotes tumor regression. Further analysis of treated tumors that had been treated with an anti-CD4 depleting antibody (CD4 DEP) showed an enrichment in TAMs as well as lower numbers of CD8+ T cells **(Fig S1g, S1h).** As CTX treated tumors always recurred after treatment was stopped (Data not shown), we then asked if TAMs mediated the eventual resistance to CTX treatment, and if so whether a treatment targeting TAMs would synergize with low-dose CTX and lead to a durable tumor response.

We implanted three independent claudin-low p53 null tumor models T11, T12 and 2151R (Fig 1a, 1b, 1c) into the mammary fat pads of immunocompetent Balb/c mice. The tumors were allowed to reach a size of approximately 5 mm in diameter and were then randomized into four treatment groups-PBS, CTX, Pexidartinib (PXB) and CTX + PXB **(Fig 1f)**. PXB is a novel small molecule inhibitor of CSF1R, which is a well-known

macrophage recruitment and differentiation factor as well as an inhibitor of C-KIT and FLT3. It recentlygained FDA approval to treat tenosynovial giant cell tumors(TNGCT)(13)and has been widely used in preclinical studies to deplete TAMs (14).
However, PXB has failed to show efficacy as a single agent, and this led us to test this agent in combination wh CTX **(Fig 1f**).

Combination treatment led to long term durable regression in two out of three tumor models namely T12 and 2151R as well as tumor stasis in T11**(Fig 1g, 1h, 1i).** Importantly, no tumors recurred in T12 while one out of eight tumors recurred in 2151R within 30 days after treatment cessation **(Fig 1j,1k)**. In contrast, all T11 tumors grew back upon treatment cessation **(Fig 1l**). Flow cytometry analysis also revealed that combination therapy treated T12 tumors had a significant enrichment of CD8+ and CD4+ T cells that expressed T central memory such as CD62l and CD127 as compared to single agent treated tumors and also an increase in effector memory T cells (CD62L+CD127+CD44+) (**Fig S1i, S1j).**

One potential advantage of using preclinical models is to improve therapeutic regimens that very often lead to serious adverse events in patients that might be irreversible and cause long-lasting damage(15) . Accordingly, we used a reduced (3.3 X lower dose) of PXB in combination with CTX as Csf1r inhibitors may elicit liver toxicity . The low-dose combination treatment also yielded a significant survival benefit for primary tumorsas compared to single agent treated T12 tumors **(Fig S1k, S1l).** This illustrates the potential efficacy of drug combinations given at less than the maximum tolerated dose, but rather at a minimal effective dose. However, this approach remains to be validated in clinical trials.

Imaging Mass Cytometry and Single cell RNA sequencing show that combination treatment can lead to an expansion of CD8+/CD4+ T cells and B cells in responsive T12 tumors
Spatial analysis done in TNBC has shown that tumors with a high number of CD8+ T cells that infiltrate into the tumor core have more favorable prognosis as compared to stroma restricted cells, indicating the importance of understanding the TIME architecture with respect to immune cells (16). Due to the unbiased selection of representative tumor areas (0.5X0.5 mm) for imaging, IMC did not prove to be the best way to quantify immune cell numbers as compared to flow or staining techniques such as IF/IHC, where you can image the entire section, especially for large tumor sections in the untreated groups, as evident in the staining for F480+ TAMs in PBS treated tumors **(Fig 2a).** However, the power of this technique enabled us to visualize and quantify the spatial interactions based on the physical distance between multiple immune cell types in the tumor microenvironment.

T12 tumors that were treated with CTX + PXB had high numbers of Cd8+/Cd4+ T cells **(Clusters 1-7)** that had were in close physical proximity with B220+ B cells **(Cluster 14)** and Cd11c+ Cd86+ Dendritic cells **(Cluster 15**). T12 tumors that were only treated with CTX had fewer interactions with between T cells and B cells and a larger group of T cell subsets **(Cluster 1,2,3 and 6)** interacted with Cd86+Cd11c+ dendritic cells and had heavy infiltrates of F480+ macrophages **(Cluster 18)** and many subsets of T cells appeared to be closely associated with these TAMS **(Fig 2d)** as well as a paucity of B220+ B cells **(Fig 2c, 2d**). This may potentially explain the reduced response to this drug as after 6 treatments. Previously we have shown a decrease in TAMs after a 3 week CTX treatment course **(Fig S1g)-**indicating the TAMs that persist after 6 treatments are resistant to CTXas a single agent.

T11 tumors that responded poorly to combination therapy were populated by Pan-CK+ Ki67+ Pdl1+ proliferating **(Clusters 12 and 13**) tumor cells interacting with sub-populations of CD8+ and CD4+ T cells**(Clusters 1-7, Fig S2a, S2b, S2c, S2c**). Additionally, flow cytometry analysis of T12 and T11 tumors showed a significantly enriched population of Cd11B+ F480+ TAMs in the poorly responsive T11 tumors (**Fig S2e)**. Studies have shown that TAMs can be recruited by tumors cells in order to escape T cell mediated killing,and we did not observe the same T cell and B cell interactions in T11 tumors as seen in **T12 (Clusters 1-7 andcluster 14, Fig2d, S2d).**

Exceptional responders to chemotherapy have shown to have high immune cell infiltrates in multiple murine cancer models and there is a need to study and characterize these cells. To further elucidate the immuneeffects of CTX+ PXB in our responsive T12 TNBC model, we performed single cell RNA sequencing(scRNA)combined V(D)J sequencing of T cell receptors (TCR) on CD45+ immune cells across all 4 treatment groups.

Uniform Manifold Approximation and Projection (UMAP) projections of the cells revealed different clusters of immune cells across the 4 different treatment groups including *Cd68*+ TAMs, *S100a8*+ Neutrophils, *Cd19*+ B cells as well as *Cd8*+ and *Cd4*+ T cells **(Fig 2e, S2f**). However, a majority immune cells from PBS and CTX treated mice clustered separately from combination treated tumors **(Fig 2f).** Upon further analysis, we observed a nearly complete depletion of *Cd*68+ TAMs and low *S100a*8+ neutrophils in the combination treated group as well as a significant expansion of *Cd4*+ and *Cd8*+ T cells. PXB alone tumors had high levels of *S100a8*+ neutrophils supporting previous studies done by our laboratories showing the accumulation of tumor infiltrating neutrophils (TINs) upon TAM depletion in treatment refractory mice **(Fig 2g)** (8). Pathway analysis using genes significantly enriched in the S100A8+ neutrophil cluster (log FC > 0.3) as compared to the other immune cells showed a significant enrichment of pathways related to granulocyte and monocyte activation andaggregation as well as pathways related to the suppression of T cell proliferation and activation **(Fig S2h**).
Further characterization of tumor infiltrating neutrophils (TINs) is required to identify targeted therapies against these cells.

Multiple studies have characterized the heterogeneity in TAMs as well as a continuum of gene expression between anti-tumor and pro-tumor TAMs (17) . The superior regression and TAM depletion observed in combination treated T12 tumors as compared to T11 tumors lead us to study the transcriptomes of TAMs as well as the bulk RNA sequencing data in both these models to see if TAM heterogeneity existed pre-treatment or was it something induced by tumors that respond poorly to chemotherapy. IHC showed an elevation of pMAPK in T11 tumors as compared to T12**(FigS2i)** and a G12V activating mutation in k*ras* in T11**(Fig S2j).**

Single cell RNA sequencing and IMC reveal phenotypically similar (Cd68+, F480+) buttranscriptomically distinct TAMs in responsive(T12) and non-responsive(T11) tumors.
There are many genetic and phenotypic similarities between the T12 and T11 p53 null tumor models. Bulk RNA sequencing revealed an enrichment for the EMT pathway and a claudin low phenotype (1) as well as an increased infiltration by TAMs. Therefore, the lack of durable response in T11 tumors came as a surprise and led to the question why these genetically and phenotypically similar models displayed a differential response. To address this question, we performed scRNA seq on untreated T11 and T12 CD45+ immune cells. TAMS clustered into 5 major clusters that included *Ly6c2*+ Monocytes, *Cd83*+ TAMs, *Irf7*+ TAMS, *Acp5*+ TAMs and *S100a4*+ TAMs Seurat clusters **(Fig 3a, 3b, S3a).** Pseudotime analysis using Monocle 3 (18) showed T11 and T12 TAMs follow distinct developmental trajectories resulting in unique populations of TAMs in T12 and T11 tumors **(Fig 3c).** This lineage splitting was orthogonally validated using Velocyto(19), a Python based tool that can map future states of cells including immune cells and it showed that a sub-cluster within the LY6C2+ monocytes was the site of the lineage split between T12 and T11 TAMs **(Fig S3b**). The baseline expression of CSF1R was significantly higher in T12 indicative that might imply a lower dependence on this signaling pathway by T11 TAMs for survival/differentiation (**Fig 3d, 3e).** IMC for T12 and T11 tumors post combination therapy showed a significantly increased population of Ki67+ proliferating cells aswell as stromal cells in T11 tumors that did not respond to therapy. Additionally, any T cells and B cells were relegated to the tumor periphery and were surrounded by F480+ TAMs that sequestered them from Ki67+ tumor cells. Studies have shown that TAMs can prevent T cell infiltration into the tumor islets, and we observedthat the optimal depletion of TAMs this in our responsive T12 tumors resulted in fewer KI67+ tumor cells and the CD8+ T cells that had infiltrated the tumor bed were in close contact with the reminder of those cells, suggesting contact dependent killing of tumor cells **(Clusters 1-7 and cluster 11, Fig 2c, 2d**). T11 post-treatment tumors had fewer interactions between these clusters **(Fig S2c, S2d, 3g)**

To further delineate the differences between T11 and T12 TAMs, we performed pathway analysis on differentially expressed genes **(logFc> 0.5, Fig 3d**) in pre-treatment T11/T12 TAMs. T12 TAMs were enrichedin

pathways related to immune activation including such as defense and inflammatory response and TAM activation markers such as C1qc **(Fig S3c)**. They also showed a downregulation of genes related to oxidative phosphorylation while T11 TAMs expressed higher levels of ox-phos related genes such as Cox1, CytB and Nd1**(Fig 3f, S3d, S3e).** Interestingly, 2151R and T12 had similar levels of these genes at a transcript level, which could indicate a degree of metabolic similarity in these responsive models. Surprisingly, T12 TAMs expressed higher levels of markers related to immunosuppressive macrophages such as Spp1**(Fig S2c)** and were more immunosuppressive in-vitro as well **(Fig S3f**). This indicates that M2 "like" T12 TAMs can also be sensitive to CSF1R inhibition and this marker could potentially be used as a stratification tool to identify patients that may respond better to these immunotherapies. Further studies are required to elucidate the role of metabolism in TAMs that survive CSF1R inhibition and whether targeting oxidative phosphorylation could be a tool to inhibit these cells.

To further understand T cell functionality in the absence of immunosuppressive tumor infiltrating neutrophils (TINs) and TAMs after combination treatment, we focused our analysis on the single cell sequencing and V(D)J data for CD8+ andCD4+ T cells in all 4 treatment groups.

Combination therapy treated T12 tumors are infiltrated by polyclonally expanded, less differentiated, exhaustion resistant CD8+ CD127+ memory T cells.

The reclustering of 2346 CD8+ T cells (see Methods) from all 4 treatment groups, revealed 6 different clusters of T cells including *Smad7*+ Naïve CD8+ T, Nfκbia CD8+ T central memory/memory precursors, *Ly6a*+(Sca-1) CD8+ T central memory, *Gzmb*+ CD8+ T effector, *Mki67*+ CD8+ T proliferative and *Lag3*+ exhausted CD8+ T cells **(Fig 4a, S4a).**CD8+ T central memory cells were greatly increased after combination therapy as compared to the other sub-populations of T cells **(Fig 4b)**. Pseudotime analysis by Monocle 3 **(See methods)** revealed that these cells were less differentiated as compared to other groups **(Fig 4c)**. CD8+ Tcm/scm cells in the combination treated group expressed high levels of markers such as Jun, Id3 and Nf bia **(Fig 4d)** which are markers of exhaustion resistance(20) , longevity(21) and are required for the maintenance of secondary lymphoid structures(22). Additionally, these cells expressed markers of early activation such as *Cd28* and *Cd69* that also control T cell differentiation **(Fig S4c).** Consistent with these results, combination treated CD8+ T cells also had a low expression of terminal exhaustion markers such as Pdcd1, Lag3 and Tigit as compared to those in untreated or single agent treated mice **(Fig 4d**). Thus, scRNA-seq analyses confirmed flow cytometry results and revealed a profound expansion of long-lived, CD8 + memory T cells upon combined PXBand CTX treatment, which may explain the durable responses for up to 30 days post-treatment seen in this group.

Most anti-tumor responses by CD8+ T cells are due to their clonal expansion triggered by specific tumor antigens that are presented by antigen presenting cells (APCs) such as CD11C+ dendritic cells and B220+ B cells(23). Macrophages can present antigens as well but cannot infiltrate lymph nodes or secondary lymphoid structures, that are usually the sites of antigen presentation. In these experiments, exhausted CD8+ T cells in PBS and CTX treated groups had higher clonality, which is consistent with studies showing monoclonal enrichment of exhausted T cells after checkpoint blockade(24). However, the T cells in the combination treated group showed a polyclonal expansion with no enrichment for a single clone **(Fig 4e, S4b)**

To functionally validate the memory status of T cells after combination treatment, we re-challenged T12 tumor bearing mice 15 days post-treatment with fresh T12 tumor chunks, that were implanted into the contralateral mammary gland. 70% of these mice showed a complete or partial rejection of these newly implanted tumors **(Fig S4d, S4e)**. This result again supports that the combined treatment establishes long-term immune memory against tumor cells. We were also able to successfully target lung metastases in a T12 tail vein model using combination treatment **(Fig 4f).** However, CTX was also able to successfully inhibit lung metastasis as compared to PBS or PXB treated mice **(Fig 4g**). Single agent PXB treatment significantly enriched the lung metastasis burden, even when compared to PBS treated mice **(Fig 4h).** These results are indicative of adistinct lung tumor microenvironment where a subset of TAMs could play a stronger anti-tumor role as compared to the TME in the mammary gland tumors.

CD4+ T helper cells as well as B cells are also known to promote anti-tumor immunity especially after checkpoint

blockade(9) and this lead us to perform further characterization these cells in our tumor model, where they also expanded upon combination treatment

CD4 T cell and B cell play an important role in mediating long term tumor regression

CD4+ T follicular helper cells and B cells have been demonstrated to promote responses to checkpoint inhibition (9) in p53 null murine models that have a high mutational burden. We observed an expansion of CD4+ T cells and CD19+ B cells after combination PTB and CTX treatment. UMAP analysis showed four different clusters*Ccr7+Cd4+* naïve, *Cd40lg+ Cd4+* T central memory, *Cd69+ Cd4+* T act and *Foxp3+*. T regulatory cells. Out of these *Cd4+* T naïve(Tn) and *Cd4+* T central memory(Tcm) cells were enriched after combination therapy while *Foxp*3+ T regs were enriched in single agent CTX treated mice**(Fig 5a, 5b**).

Pseudotime analysis without using defined root points showed that programmatically the CD4+ T naive population was the least differentiated cell cluster followed by the Tcm cells further along the trajectory **(Fig 5c, S5b)**. The transcriptomic analysis of these two subclusters did not show a high number of unique genes per cluster-with the genetic heterogeneity lying more in the differences of gene expression level than gene type. The CD4+ Tn cells expressed common naïve markers such as *Ccr7*, *Sell*, *Lef1* and low levels of *Cd69* which is typically a marker of early T cell activation **(Fig 5d**). However, CD+ Tcm cells enriched after combination treatment has increased expression of *Cd69* and other markers associated with T cell longevity and survival such as *Id3/Fos/Jun***(Fig 5e)**.This supports recent studies that have shown that the transcriptomes of Tn and Tcm cells derived from patients do not represent two discrete states between these two populations but rather show a continuum of gene expression(25).

Additionally, V(D)J analysis revealed a polyclonal expansion of these subsets as well **(Fig S5a)**
CD4 T cm cells after combination treatment also displayed increased expression of the CD40 ligand(lg), which is a member of the Tumor Necrosis Factor (TNF) family of ligands **(Fig 5e)**. CD40lg is expressed primarily on activated T cells. However,it is also present on B cells, dendritic cells, and macrophages. The receptor for CD40lg is CD40. It was first discovered on B cells but is also expressed on other antigen presenting cells such as dendritic cells.
CD40/CD40lg is essential for the survival of antigen presenting cells including B cells where it can lead to the maturation of B cells, increase their ability to effectively present antigens to T cells and form germinal centers. To determine if there was a relationship between the *CD40lg* T cm cells and the *Cd19+* B cells that expanded after combination treatment we performed ligand receptor analysis for all four treatment groups **(Fig 5f).** Interestingly-we identified a unique interaction between CD4 T cells and B cells in the combination treated group which was CD40lg and TRAF3. Previous studies have implicated TRAF3 in the inhibition of canonical and non-canonical NF- B signaling as well as a reduction in CD40 transcript. However, this effect is thoughtto be cell type specific. Other studies have shown that TRAF3 can mediate class switching which is essential for B cells to proliferate and generate a diverse antibody repertoire directed towards multiple tumor antigens (26) Based on these results we then decided to study the reciprocal interactions between B cells and CD4 Tcm cells in the singly and combination-treated mice.

Activated B cells expand after combination immunotherapy and are the main antigen presenting cellsto CD4+ T memory cells with tertiary lymphoid structures
Single cell RNA sequencing data for all four treatment groups for CD19+ B cells revealed three discrete subclusters including *Cd19+* B cells, *Cd86+* activated B cells (ABCs) that expressed high levels of Cd40 and Germinal center (GC)-like B cells that expressed GC markers such as *Bcl6(***Fig 6a, S6a).** ABCs were enriched after combination treatment **(Fig 6c)** and these cells had increased expression of CD40 and Rel as compared to the naïve B cells **(Fig 6a,S6a**). Rel is a member of the NF- B family of transcription factors and is essentialfor the long-term survival of activated B cells (ABCs). Trajectory analysis of B cells showed that activated B cells followed a distinct maturation trajectory as compared to GC-like B cells that were enriched after singleagent PXB treatment or in untreated mice **(Fig 6b, 6c**). These B cells also expressed imunnoglobulin transcript genes such as Ighm and Ighd **(Fig S6a),** however this remains to be validated at a protein level.

Besides CSF1R, PLX3397 has also been shown to inhibit FLT3, which is an important dendritic cell (DC) maturation factor. We did not observe an expansion of antigen presenting DCs after combination treatment however, pathway analysis of ABCs showed increased expression of antigen presentation pathways to both CD8+ and CD4+ T cells indicating that after combination treatment-B cells are the chief antigen presenting cells instead of dendritic cells or macrophages **(Fig 6d**). Reactome analysis showed an upregulation of NF- B survival signaling indicating the CD40LG-TRAF3 interactions are not inhibitory in this context **(Fig S6c**). These data indicated that both CD4+ T cells and CD86+ activated B cells are essential for long-term response to CTX and PLX3397 in our models.

Consistent with this long-lasting durable response to combination treatment, we observed the significant presence of tertiary lymphoid structures (TLS) in the tumor beds of treated mice bearing regressed T12 tumors6 weeks post-treatment **(Fig S6e**) as compared to the untreated or single agent tumors that were harvested 7 days post-treatment due to the size of these tumors exceeding IACUC recommendations. We also observed TLS at the original site in mice that completely rejected T12 tumor rechallenge and they expressed endomucin, which is a component of heavy endothelial venules(27)-a known TLS marker **(Fig S6d).** Since long lasting TLS have been implicated in improved responses to checkpoint blockade therapy, we performed IMC and observed highly significant interactions between subsets of CD8+/CD4+ memory T cells **(Clusters 1-5)** and B220+ B cells **(Clusters 8 and 9)** and avoidance of CD11b+ F480+ macrophages and Ly6C+ monocytes **(Clusters12 and 13, Fig 6e, 6f)** . Using markers obtained from our scRNA seq analysis to further delineate B cell heterogeneity-we identified 2 B cell sub- populations which were B220+CD86+ and B220+CD86-**(Clusters 8 and 9**) to see whether a certain B cell subset preferentially interacts with T cells in TLS.

We observed significant interactions between B220+ Cd86+ B cells and Cd8+/Cd4 + Cd44+ T cells**(clusters 1,2,4,5 with cluster 9, Fig 6g)**. CD44 is a known T cell memory marker along with Cd62l, but we did not observe a high number of these cells in our scRNA seq data while the mice were on treatment(**S5c)** and only identified these cells in TLS, 30 days post therapy **(Fig 6e, 6f).**This could possibly be a subset of T cells that expand after combination therapy and are long lived/help in promoting long-term tumor regression. Cd4+Cd44+ T cells **(Cluster 4)** interacted with B220+Cd86+ B cells**(Cluster 9)** but had no significant interactions with Cd11d+ Dendritic Cells**(Cluster 10, Fig 6g)**. This indicates the possibility that antigen presenting B cells can persist at least 6 weeks post-treatment and are the main APCs in long-lasting TLSs after combination therapy. Interestingly, one of the top pathways identified in the GO analysis of activated B cells in combination treated mice was related to lymphoid organ development **(Fig 6d).** Further studies are needed to understand the mechanisms by which B cells can promote the formation of anti-tumor tertiary lymphoid structures.

Activated B cell signatures correlate with pCR in multiple datasets of TNBC patients undergoing neoadjuvant chemotherapy.

To test the clinical relevance of immune cell scRNA seq subsets, we derived a signature that is comprised of differentially expressed genes **(logFc >0.03, Supplemental Excel File 1)** from the activated Cd86+ B cells (ABC) as compared to the other B cell sub-populations which is included in Supplemental table S1. We applied this signature to multiple clinical datasets for TNBC patients treated with neoadjuvant chemotherapy (NAC) including GSE123845 and GSE41998. Transcriptomic data for these patients was available pre and post-treatment.We analyzed the correlation of markers that identify all B cell populations such as CD19 and CD20 and observed a significant association of these markers with complete responses to NAC in all breast cancer subtypes **(Fig 7a**) as well as TNBC alone **(Fig 7b).** While our ABC signature did not show this association when used as a single variable, multivariate analysis using this B cell signature with CD19/CD20 B cell markers resulted in a clear correlation(R=0.569) between these two factors in relation to pathological complete response(pCR**) (Fig 7a, 7b, 7c).** This observation suggests that B cells found in patients undergoing pCR are predominantly enriched with the activated Cd86+ subset, which highlights their importance in improved tumor

response. In contrast, in tumors exhibiting resistance, ABC appears to be depleted from the general B cell population as indicated by the negative correlation with CD19 and CD20. Interestingly, an intermediate level of correlation was observed for tumors with partial responses, further supporting the hypothesis that the proportion of ABC among all B cells may determine responses to cyclophosphamide-containing chemotherapies. We also used the transcriptomic signature for T12 TAMs as compared to T11 TAMs **(Fig 3d)** and observed that this TAM signature is associated with B cell abundance especially in patients sensitive to AC (**Fig 7d**).
We also examined an additional TNBC dataset (GSE123845) and again observed that universal B cell markers such as CD19 and CD20 were significantly enriched in patients that underwent pCR. In addition, further multifactorial analysis revealed that the activated B cell cluster-derived signature significantly correlated with pCR. In contrast total infiltrating lymphocytes (TILs) did not show this relationship **(Fig 7Sa, 7Sb, 7Sc).**

Discussion

Triple negative breast cancer is a highly aggressive malignancy with higher rates of occurrence in young as well as African American women. Current treatment usually employs cytotoxic chemotherapies, with immune checkpoint inhibitors being newly approved for use in TNBCs (28). While certain clinical trials have reported positive outcomes for TNBC including T cell activating agents such as checkpoint inhibitors, the response rates in these patients vary and clearly more refined therapies are needed to improve patient survival especially in the metastatic setting. The immune microenvironment in TNBC has been suggested to play a critical role in patient response. Accordingly, our laboratories have extensively characterized the immune microenvironments of various GEM TNBC models including those that are either neutrophil enriched or macrophage enriched and have begun to decipher the molecular mechanisms behind how different immune cells are recruited to both the primary tumor and metastasis.

In this study, we performed an in-depth analysis of claudin-low TNBC models using the latest single cell RNA and VDJseq techniques, as well as sophisticated imaging technologies such as Imaging Mass Cytometry. These tools have provided new insights into changes in the immune microenvironment before and after combination treatment with both chemo- and macrophage- targeting therapies. Surprisingly, these studies revealed a subtle heterogeneity that exists between genetically and phenotypically related models that appear to be enriched for similar immune cells types such as macrophages and pathways such as the EMT pathway. The models used in this study, namely T12, T11 and 2151R have shown varying responses to a low dose CTX and a FDA approved Csf1r inhibitor. While T12 and 2151R models display a dramatic response leading to as complete long-lasting regression of the primary tumors upon treatment cessation, T11 tumors display stasis while undergoing treatment but recurred rapidly once treatment cessation.

Tumor associated macrophages classically have been classified as either M1 and M2 type macrophages with activating and immunosuppressive functions, respectively although more recent studies have illustrated that this designation is overly simplified and there is a much more complex spectrum of activities. Studies thathave performed single cell RNA sequencing on patients with colorectal cancer have identified subsets of C1QB+ macrophages that have differential sensitivity to CSF1R blockade(29) . These results are consistent with our data that shows T12 TAMs have high C1QB, express higher levels of Csf1r and are more sensitive toPLX3397. Conversely the T11 TNBC model is infiltrated by highly metabolically active TAMs that are marked by the expression of S100A4 and ACP5. Additionally, while T12 TAMS appear to have an increase of the cytokine metabolism pathways and genes related to glycolysis, T11 TAMs seem to depend upon oxidative phosphorylation for their energy needs. This suggests that further studies done using inhibitors of oxidative phosphorylation and the electron transport chain in this model are warranted. For example, a small molecule inhibitor of oxidative phosphorylation-IMT1B-has shown some efficacy in models of human ovarian cancer(30) and could potentially be an interesting drug to combine with immunostimulatory chemotherapy. This may target this subset of TAMs and potentially might result in a durable long-term tumor response. Another drug is Venetoclax- a known inhibitor of anti-apoptotic molecule Bcl2(31) . Recent studies have shown its inhibitory effects on oxidative phosphorylation and it would be interested to see its effects on oxidative phosphorylation dependent TAMS. The present study identified mouse models that will provide invaluable tools to study TAM heterogeneity in the future. Furthermore, the publicly available scRNA seq datasets of T11 and T12 tumors provide a resource for the scientific community to explore TAM heterogeneity in greater detail.

Depletion of TAMs within the tumor microenvironment coupled with a low dose of immunostimulatory chemotherapy was able to elicit durable tumor regression and an expansion of polyclonal long-lived central memory T cells in certain TAM infiltrated models. These cells persist for long periods of time at the primary tumor site after tumor regression and they may also facilitate tumor rejection upon rechallenge.

Another unexpected observation is the presence of Tertiary Lymphoid Structures within the primary tumor site that persist post treatment. While these structures have been implicated in improving the prognosis for patients that respond to checkpoint inhibition, they are usually thought to be transient and have not been studied in detail in mouse models of TNBC. We have shown that TLS co-infiltrated by antigen-presenting Cd86+ B cells and Cd4+ Cd44+memory T cells can persist within the tumor site for extended periods of time post-treatment and may be important in achieving long term disease control. We have also shown that signatures derived from the Cd86+B cell sub-population have shown a clear correlation with TNBC patients treated with NAC and exhibiting pCR in multiple datasets. Additional analysis revealed that TILs only correlate with our B cell signatures in patients that have achieved pCR, indicating the important role of B cells within total TILs in achieving pCR for TNBC patients. No such correlation was seen in patients that did not achieve pCR. One hypothesis could be that T12 macrophages help tumor cells escape B cell-mediated immunosurveillance. Therefore, tumors evolve to keep a balance between this type of macrophage and B cells. Anti-macrophage treatment might be especially usefulin this case because it will abolish T12 macrophages and unleash B cell-mediated immunity.

Future studies using these models may help elucidate the mechanisms by which tumors of the same subtype differentially respond to treatment. A higher proportion of treatment-resistant circulating stem cells may explain the failure of CD8+ memory T cells to mount a strong anti-tumor response. Further studies are also required to elucidate the mechanisms that account for the phenotypic switch following the initial recruitment of macrophages to pathways that recruit immunosuppressive neutrophils. A more detailed analysis of the tumorsthat recur in the primary and metastatic sites is also needed. These preclinical studies will need to be extended to longitudinal studies in patients with new therapeutic combinations that can target potential immunological transitions to better improve long term progression free survival.

This study also further highlights the need to further understand the heterogeneity in B cell sub-populations. Future studies need to carefully examine their role in TNBC patients that do not respond to chemotherapy and to develop targeted treatments that can modulate B cell functionality like studies being done in TAMS. These results highlight the need to integrate newer techniques such as single cellRNA sequencing in combination with high dimensional imaging data to analyze patient samples in order to enhance our understanding of TILS and therapeutic response.

Author Contribution

S.S., C.M.P., X.H.F.Z., and J.M.R. conceptualized the study, designed the experiments and wrote the manuscript. S.S. performed the experiments. C.H., S. A., D.P., Y.G., N.Z., and I.B., assisted with the mouse experiments and acquisition of data. L.C., Y.X., and S.L performed IMC staining and analysis. S.S., N.L., I.B., Y.W.W., Y.S., J.S., Z.L., and D.H. analyzed the bioinformatics data and discussed the project direction. S.S.,and X.H.F.Z.,analyzed clinical trial data.

Acknowledgements

We would like to acknowledge Dr. Xi Chen for his help reviewing the manuscript, and Ipshita Thakur for illustrating the mice used in the treatment schemes. We would like to thank Jonathan Shepherd for his help with bioinformatic analysis. These studies were supported by grants NCI-CA148761(C.M.P and J.M.R.), Breast Cancer Research Foundation, NCI CA151293, US Department of Defense DAMD W81XWH-16-1-0073 and W81XWH-18-1-0574, Susan G. Komen CCR14298445, and McNair Medical Institute (X. H.-F. Z.) CPRIT grant RP160283(S.S.), the Dan L. Duncan Comprehensive Cancer Center (NCI: P30: CA125123) and Pathology Core of the Lester and Sue Smith Breast Center. This project also was supported by the Advanced Technology Cores at BCM: Genomic and RNA Profiling Core (NCI: CA125123), Single Cell Genomics Core,Cytometry and Cell Sorting Core (CPRIT-RP180672), and Integrated Microscopy Core (NIH: DK56338 and CA125123; CPRIT:

RP150578 and RP170719).

Declaration of Interests

C.M.P is an equity stock holder and consultant of BioClassifier LLC; C.M.P is also listed as an inventor on patent applications for the Breast PAM50 Subtyping assay. The others authors declare no competing interests.

Methods

Cell Lines

T11 and T12 cell lines were generated in the Rosen laboratory from primary T11 and T12 tumors by selectionof epithelial cells expressing the neomycin cassette in G418.and cultured in DMEM/High Glucose with 10 % FBS, 100 IU ml^{-1} penicillin/streptomycin (Lonza), 5 µg/ml insulin, 10 ng/ml mouse EGF, and AA) and hydrocortisone. Cells were maintained in a humidified incubator at 37°C with 5% CO2. Mycoplasma testing was carried out on the cell lines once a month.

Animals Studies

All animals were used according to a protocol approved by the Institutional Animal Care and Use Committee at Baylor College of Medicine. Female 5-6-week-old BALB/c mice were ordered from Envigo Laboratories and experiments were carried out in age matched animals. Female 5-6-week-old NSG mice (NOD.Cg-Prkdc scid il2rg tm1 Wjl/SzJ) (Stock no 005557) were ordered from Jackson Labs.

Mice were house in the TMF Mouse Facility at the Baylor College of Medicine in SPF/climate-controlled conditions with 12-hour day or night cycles. They were supplied with fresh chow and water from an autowater system continuously.

Mammary fat pad injection

The generation of T12, T11 and 2151R tumor models has been described and characterized previouslyand tumor chunks were stored in liquid nitrogen for long-term storage in FBS + 10% DMSO. Prior to surgery, tumor chunks were thawed and washed in PBS. Tumor chunks were implanted directly into a small cavity in the mammary fat pad. Mice were monitored for tumor growth and were randomized into treatment groups when the tumors were approximately 5 mm in diameter.

In-vivo treatment Studies

Cyclophosphamide (Sigma Aldrich, PHR1404-1G) was resuspended in sterile PBS(Lonza) and injected i.p at the concentration of 100 mg/kg, once a week for the entire treatment period and the control mice were injectedwith the same volume of sterile PBS.

PLX3397 was obtained from Plexxikon, Daichii Sankyo and was added to a chow made by Research Diets. Mice were fed the chow ad libitum. The drug concentration in the chow was 275 ppm in most of the experiments described which corresponds to 5 mg/kg per mouse except for the low-dose experiments with a concentration of 75 ppm. Control mice were given the same chow without PLX3397. Mice were weighed and monitored for signs of drug toxicity weekly. Tumors were measured using calipers 3 times a week for the duration of the treatment.

In-vivo T cell depletion studies
Mice were injected i.p. with anti CD4(100 ug, BE0003-1) or anti CD8(150 ug, BE0061) antibodies obtained from Bioxcell Laboratories, twice times weekly. Optimal antibody concentrations were obtained from previous validation experiments. This was repeated during the entire treatment course.

Tail vein injection
Female 5-7-week-old BALB/c mice were injected with tumor cells dissociated from fresh T12 mammary tumors. Cells (200,000) in sterile PBS were injected in per mouse using a 27-gauge syringe. Mice were randomized into treatment groups at day 10 post injection and were given 3 weekly treatments of CTX and PLX3397 chow ad libitum, following which the mice were sacrificed and the lungs were collected for further analysis.

T cell isolation and In-vitro immunosuppression assay
Spleens were harvested from 8-week-old JEDI mice and physically dissociated using a scalpel. Splenocytes were filtered through a 70- m cell strainer. Red blood cells were lysed using RBC lysis buffer (#B4300062518TN, Tonbo Biosciences). CD3+ T cells were enriched using negative selection of biotinylated antibodies B220, CD11b, CD11c, and Gr-1 (#559971, BD Pharmingen) and magnetically sorting using EasySep Mouse Biotin Positive Selection kit (#18559, Stemcell). CD3+ T cells were activated using a 1:1 ratio Dynabead Mouse T Activator CD3/CD28 (#00775477, Thermo Scientific) for 72 hrs in T cell media containing RPMI 1640 (VWR), 5% heat inactivated FBS, 55 m ß-mercaptoethanol, and 5ng/ml IL-2(# 202-IL-050/CF, R&D Systems). Activated CD3+ T cells were isolated from Dynabead Mouse T Activator CD3/CD28 (#00775477, Thermo Fisher) using negative selection. T12 unlabeled and GFP labeled cell lines were seededat a density of 2500 cells per well in a 96-well plate. After 24 hrs, T cells were added at a 10:1 effector/target ratio with 10,000; 1,000; 100; 10; 1; 0 m of phosphoramide mustard (#M123069, MuseChem). Each condition was run in triplicate. The conditions include co-culturing with T cells and drug, and wells with drug alone. The plate was incubated in an Incucyte (Essen) and fluorescence and phase images were taken every hour for 48 hrs. The analysis was run using Incucyte S3 software and graphed using Graphpad Prism 8.

For co-culture experiments with tumor associated macrophages, TAMS were isolated from fresh T12 or T11 tumors using the marker F480 by FACS sorting. They were seeded at a 1:1 ratio with the T cells in the media mentioned above with 20 % tumor cell conditioned medium. The cells were kept in culture for 72 hours following which the T cells and tumor cells were separated and analyzed by flow.

Tissue staining
Primary tumor and lung tissue were fixed in 4% paraformaldehyde overnight and transferred to 70% ethanol for long-term storage. The tissue was embedded in paraffin blocks by the Breast Center Pathology Core at Baylor College of Medicine. IHC was performed according to Rosen Lab protocols (https://www.bcm.edu/research/labs/jeffrey-rosen/protocols).
Primary antibodies used were ordered from Abcam-anti-CD4(EPR19514), Anti-CD8a (YTS169.4), S100A8(EPR3554), F480(CI: A3-1) or eBioscience B220(RA3-6B2). Biotinylated secondary antibodies were ordered from Biolegend.

Flow Cytometry
Tumors were dissociated using the MACs mouse tumor dissociation kit(Miltenyl Biotec) and suspended in PBS+1% FBS. The cells were incubated in blocking buffer containing 1:200 CD16/32(clone 93, eBioscience) for 30 min on ice. They were subsequently stained by fluorescent-conjugated primary antibodies at previously validated concentrations for 1 hr on ice. Following three PBS+1 % FBS washes, the cells were resuspended in ice cold PBS or fixed in 1 % PFA for immediate acquisition on the LSR Fortessa at the Baylor College of Medicine FACS and Cell Sorting core. Data was further analyzed using FlowJo Software version 10.0.

The following antibodies against mouse antigens were used: anti-CD3ε (145-2C11), anti-CD4 (GK1.5), anti-CD8 (53-6.7) (all from eBioscience); anti-B220 (RA3-6B2), anti-CD11b (M1/70)), anti-CD45 (30-F11), anti-F4/80 (BM8), anti-Ly6G(IA8)(all from Tonbo); anti-CD127 (SB/199, BD Biosciences), anti-CD44 (IM7, BD Biosciences), anti-CD62L (MEL14, Biolegend), Anti-KI67(16A8, Biolegend), anti-CSF1R(AFS98, Biolegend),

anti-KLRG1(2F1, Biolegend).

IMC Staining and Quantification

IMC staining and data processing was done at the Houston Methodist Immuno- Monitoring Core. Metal conjugated antibodies were ordered from Fluidigm or validated and conjugated to metals using the MaxPar antibody conjugation kit (Fluidigm). The antibodies used were suspended in BSA and azide free buffers and after conjugation they were diluted in Candor PBS Antibody Stabilization solution (Candor Bioscience) for longterm storage at 4°C.The antibodies used and metal conjugates are listed in Supplementary Excel File 2.

Paraffin embedded tumor tissue samples were sectioned onto slides with each section having a thickness of 5 um. The sections were baked at 60ºC overnight, deparaffinization was performed in xylene and the sections were rehydrated in a graded series of ethanol solutions (90%, 80%, 70% and 50% for 10 min each. Antigen retrieval was performed using 1 µM sodium citrate buffer (pH 6) for 20 min in a heated water bath. Blocking buffer containing 3% bovine serum albumin in tris-buffered saline (TBS) was added to each section and the slides were incubated at R.T for 1 hr. The sections then were incubated in metal conjugated primary antibodies at 4ºC overnight. The next day, samples were washed 4 times in TBS-T following which they were stained with Cell-ID Intercalator (Fluidigm) for nuclear staining. Three random sections per tumor section measuring 0.5 X 0.5 mm were ablated and imaging mass cytometry data were segmented by ilastik and CellProfiler. Histology topography cytometry analysis toolbox (HistoCAT) and R (Version 1.2.5042) were usedto analyze the images and perform clustering and neighborhood analysis.

qPCR Protocol and primer sequences

RNA was isolated from primary mouse tumor tissue using TRIzol reagent (# 15596018, Thermo Scientific). Total RNA was then reversed transcribed into cDNA using the RT2 first-strand kit (#330401, Qiagen). Realtime quantitative RT-PCR was carried out in triplicates utilizing the amfiSure qGreen Q-PCR Master Mix (#Q5602005, GenDEPOT) using a StepOnePlus real-time PCR system (Applied Biosystems, Foster City, CA, USA) and analyzed using the comparative Ct method ($2^{-\Delta\Delta Ct}$) with GAPDH as the housekeeping reference gene. The primers utilized are listed in the table below.

Gene Name	**Primer Sequence**
Nd1-F Mouse	ACGCAAAATCTTAGGGTACA
Nd1-R Mouse	GAGTGATAGGGTAGGTGCAA
Cytb-F Mouse	TCCTTCATGTCGGACGAGGC
Cytb-R Mouse	AATGCTGTGGCTATGACTGCG

RNA sequencing analysis

Tumor sample mRNA quality was measured using the Agilent Bioanalyzer and libraries for mRNA-seq were made using total RNA and the Illumina TruSeq mRNA sample preparation kit. Paired end (2x50bp) sequencing was performed on a Illumina HiSeq 2000/2500 sequencer at the UNC High Throughput Sequencing Facility. Consequential fastq files were aligned to the mouse mm10 reference genome using the STAR aligner algorithm . Ensuing BAM files were sorted and indexed using Samtools and quality control was performed using Picard. Transcript read counts were determined was performed using Salmon. The RNA-seq data was processed and normalized as published (2). Gene expression signatures were calculated as the median expression of all the genes in the signature as published. Non treated tumors from existing published geneexpression data were used for this study (7) (and can be accessed on the Gene Expression Omnibus (GEO) under accession GSE124821. All the bulk RNA sequencing data for T12, T11 and 2151R is available under accession

GSE173260.

Single cell isolation and scRNA sequencing analysis

Tumors were dissociated as described previously and CD45+ cells were isolated from tumors using the Miltenyi Magnetic Enrichment Kit or FACS sorting. Fresh cells were suspended in PBS and library preparationwas carried out by the Single Cell RNA Sequencing core at Baylor College of Medicine using the 10X Genomics Chromium RNA seq 5 prime Kit. The samples were sequenced at the Genomic and RNA Profiling Core at Baylor College of Medicine on Nextseq 500 or NovaSeq 6000 sequencing machines from Illumina.
Raw data has been uploaded on GEO under accession number GSE165987.

Single-cell data sequencing and processing

Cellranger Count and vdj

Fastq files with range of 26-28bps for R1 and 89-96bps for R2 were processed using the Cell Ranger Single Cell Software Suite provided by 10x Genomics, V3.0.2. Reads were aligned to mouse genome (mm10) whichis available on cellranger's website http://cf.10xgenomics.com/supp/cell-exp/refdata-cellranger-mm10-3.0.0.tar.gz. Filtered gene-barcodes matrices that passes the default cellranger threshold for detection were used for further analysis. We obtained an average of 1803 unique genes per cell with a median of 1413 and an average of 7668 unique transcripts per cell with a median of 4147 which is comparable to similar scRNASeq studies. For the VDJ samples, the fastq files were processed using the cellranger vdj pipeline and the reads were alligned to the GRCm38 reference genome which is also available on cellranger's website at http://cf.10xgenomics.com/supp/cell-vdj/refdata-cellranger-vdj-GRCm38-altsensembl-2.2.0.tar.gz.

Data Processing

The first analysis which studies T cells consisted of four samples: 16805(PBS), 17746(CSF1R), JR20876(Combination) and JR20877(CTX). The second analysis studying Myeloid cells consisted of four samples: T12(16800 and 16805) and T11(Gao1 and Gao2) mice models. All downstream analysis were performed using Seurat R package, V3.1.3 and Monocle3_0.2.0.

Seurat

Downstream analysis of the RNA data was performed using the Seurat R package, V3.1.3 (32). Cells with greaterthan 10% mitochondrial counts were removed. Outlier cells with greater than 40,000 were removed. All rps, rpl, mt and gm genes were also removed. The data was normalized and the top 3000 genes with the highest residual variance were selected as the highly variable genes seurat's SCTransform. SCTransform also filters out genes that are present in less than 5 cells. This resulted in 31167 cells and 15976 genes from 36198 cells and 31053 genes for the T Cell study whereas it was 19352 cells and 15365 genes from 21325 cells and 31053 genes for the Myeloid study. The PCA scores were computed using Seurat's RunPCA function and the clusters were identified using first 30PCs with a resolution of 1.2 for the T Cell study while the Myeloid study uses the same number of PCs but with a resolution of 0.8. The UMAP projection were for both studies were generated using the first 30PCs with a default parameter of 0.3 minimum distance and k = 30 neighbors.
T Cells study samples were further split into CD4 T Cells and CD8 T Cells. CD4 T Cells were subset based on Cd4 > 0.5 and Cd3e >1 while CD8 T Cells were subset based on Cd8a > 0.5 and Cd3e > 1. Cells that intersect between the CD4 and CD8 T Cells subset were removed. This resulted in a subset of 3859 unique CD4 T cells and 2346 unique CD8 T Cells and the raw counts with the original number of genes of 23393(rps, rpl, mt and gm genes were removed). SCTransform was performed on both the CD4 and CD8 T Cell subset which resulted in 3859 cells and 11758 genes while it was 2346 cells and 11918 genes for CD8 T Cell. For CD4 T Cells, the PCA scores were recalculated and the clusters were reidentified using the first 30PCs with a resolution of 1.5. For CD8 T Cells, the the clusters were identified using the first 50 recalculated PCs resolutionof 1.0. The UMAP projection were regenerated using the first 30PCs for CD4 T Cells while CD8 T Cells used the first 50PCs. The other UMAP parameters remained unchanged with a default parameter of 0.3 minimum distance and k = 30 neighbors.

CD19 B cells were subset based on Cd19 > 0.5 on the SCT assay of the T Cell samples which resulted in 630 cells. SCTransform was performed on the raw counts of 23393 genes. This output a Seurat object with 630 cells and 10509 genes. PCA scores were again recalculated and the clusters were reidentified using the first 30 PCs with the default resolution of 0.8. The UMAP projections were recomputed with default parameter of 0.3 minimum distance and k = 30 neighbors.
Itgax D cells were selected by subset Itgax > 0.5 from the SCT assay of the T Cell samples. The output of the subset is 1510 cells. SCTransform was performed on the raw count of 23393 genes and this resulted in 1510 cells and 12143 genes. PCA scores were recomputed and clusters were reidentified using the first 30PCs witha default resolution of 0.8. The UMAP projections were reinitialized with the default parameter of 0.3 minimum distance and k = 30 neighbors.
For the Myeloid study, Macrophages and Monocytes cells were subset based on the SingleR Immgen annotation (33) that is explained below. 15718 cells were subsetted with the raw counts of theoriginal 23393 genes. The data is renormalized using SCTransform which outputs 15718 cells and 14688 genes. The PCA scores were recomputed and 30PCs were used to reidentify the clusters with a resolution of 0.8. The UMAP projection were obtained using the first 30PCs with the default parameter of 0.3 minimum distance and k = 30 neighbors.

Annotation

For CD8 T Cell, the clusters were manually annotated with the following annotation: Nfkbia+ CD8+ Tcm (Cluster 0, 6, 7, 9, 11 and 13), Ly6a CD8+ Tcm (Cluster 2), Smad7+ CD8+ Tn (Cluster 1 and 14), Gzmb+ CD8+ Teff (Cluster 4 and 5), Mki67+ CD8+ Tprof (Cluster 12) and Lag3+ CD8+ Tex (Cluster 3and 10).
As for CD4 T Cell, the clusters were manually annotated as : CD4 T naïve (Cluster 0,3,4,7,9 and 10), CD4 T cm (Cluster 1,5,8,13 and 14), Foxp3+ Tregs (Cluster 2 and 12) and CD4 T act (Cluster 6 and 11).For the CD19 B Cells, Cluster 4 and 5 were removed while the other clusters were annotated as follows: Cluster 0 and 2 - FO B Cells, Cluster 1 – Activate GC B Cells and Cluster 3 - Plasma Cells
Clusters of Myeloid study and D Cells were annotated using the new SingleR, V1.0.5 which is available at https://bioconductor.org/packages/release/bioc/html/SingleR.html. The Immgen reference which has a collection of 830 microarray samples - with 20 main cell types and 253 subtypes – was used as the reference to annotate the dataset. The SingleR annotation were used to subset Myeloid cells in the Myeloid study. After the subset, the clusters were reinitialized and the UMAP were recomputed. This resulted in 20 clusters. Cluster14 and 19 were removed due to being outliers and the rest of the clusters were annotated as : CD83+ TAMs (Cluster 1,7,10,12,13,15,17 and 18), S100a4+ TAMs (Cluster 2 and 5), Ly6c2+ Monocytes (Cluster 3 and 9), Acp5+ TAMs (Cluster 4 and 11) and Irf71+ TAMs (Cluster 0,6,8, and 16).

Differentially Expressed Genes

Differential expression test was done using the Wilcoxon Rank Sum test which is the default of Seurat's FindMarkers function for all genes that has not been filtered out. Logfc.threshold = 0 and min.pct = 0 parameters were used. The test was conducted for both the Seurat clusters and the celltype clusters annotated by SingleR. Three extra comparison were made for CD4 and CD8 T Cells which were Combination vs CSF1R, Combination vs CTX and Combination vs all.

Pseudotime Analysis

The pseudotime trajectory of CD4 and CD8 T cells as well as Macrophages/Monocytes cells were obtained using the monocle 3 pipeline, V3.0.2. For all three analyses, there was a further subset based on the Seurat clusters or SingleR annotation. We filtered out Monocytes from CD8 T Cells, B Cells from CD4 T Cells and for the Myeloid study, Cluster 14 and 19 were filtered out due to being outliers. The monocle3 pipeline was customized to utilize the already computed Seurat's UMAP embeddings. The partitions that were determined by Monocle were manually set to one to have a continuous lineage. The branches and leaf point index numberwere manually modified to show sequence.

RNA Velocity

The Cellranger bam files were re-sorted using samtools. The loom file for each sample were obtained by running the velocyto python script(V0.17.17) with the masking parameter. The masking gtf file was downloaded from the UCSC genome browser with the RepeatMasker track selected. The loom files were merged. The Velocyto-Seurat wrapper(velocyto.R V0.6) was then used to obtain the RNA velocity. The RNA velocity were then plotted on the computed UMAP from the analysis above.

Ligand Receptor Analysis

Significant ligand-receptor (LR) pairs were identified using the same method as as previously described (34, 35). We focused our analysis on the 2422 LR pairs published in these studies as well. A ligand or receptor is considered expressed if theSCT-normalized data is 0.5 in at least 10% of the cells. If a ligand or receptor is not considered expressed, theexpression value will be set to zero. P-values were generated from 1,000 permutations with random shuffling the cell labels. A LR is considered significant if the interaction score is at least 2 and $p < 0.01$

Patient Data Analysis

We scored the association of B cell activation signature and T11 vs T12 macrophage signature with outcomes in triple negative breast cancers using RNA-Seq data using a recently published TNBC patient data set, GSE41998 (36) and GSE123845 (37). The data were downloaded from GEO either as raw count matrix or as normalized data preprocessed using the BETSY platform (38) using a STAR aligner (39) and HTSeq-Count (40) to determine read counts . The raw counts were transformed to log 2 scale. A z-transformation was then performed across all genes of each sample. The signatures were scored using the average of constituent gene values. Associations were assessed using Pearson correlations and the corresponding p values were computed according to Student's t tests.

Pathway Analysis

Pathway analysis was carried out on subsets of CD68+ myeloid Cells in T12 and T11 tumors. Differential Gene Expression was obtained using the Wilcoxan Rank Sum Test, logFc > 0.5 using R studio. Signatures obtained were labeled T12vsT11 and T11vsT12 signatures (Excel, Table 3) and they were used for pathway analysis and patient data analysis in the paper. GSEA analysis (41) was used to determine if pathways were statistically different in the tumor models using FDR < 0.1 as cut off . Gene signature pathways related to metabolism were downloaded from MSigDB (42) . GO and reactome analysis was performed analysis was performed using murine specific biological pathways lists downloaded from the Gene Ontology Database and Fisher's exact test was used to determine the significance of the pathways.

Statistical methods.

Sample sizes were not predetermined for treatment studies and are denoted in the figure legends. Each in-vivo experiment was repeated at least 3 times with independent cohorts of mice. Data was show as the mean +- the SEM. All in-vitro experiments were repeated 3 times independently. Each condition was done in biological replicates and the combined data was used to determine the P values.

Statistical analysis was carried out using Graphpad Prism or R Studio (Version 1.2.5042). Statistical significance for tumor volumes was carried out using unpaired paired t-tests or two-way ANOVA (Analysis of variance) with a p value lower than 0.05 being considered significant. Survival analyses were evaluated by Kaplan-Meier curves and the log-rank (Mantel-Cox) test.

References

1. Herschkowitz JI, Zhao W, Zhang M, Usary J, Murrow G, Edwards D, Knezevic J, Greene SB, Darr D, Troester MA, Hilsenbeck SG, Medina D, Perou CM, Rosen JM. Comparative oncogenomics identifies breast tumors enriched in functional tumor-initiating cells. Proc Natl Acad Sci U S A. 2012;109(8):2778-83. Epub 2011/06/03. doi: 10.1073/pnas.1018862108. PubMed PMID: 21633010; PMCID: PMC3286979.
2. Lin EY, Pollard JW. Tumor-associated macrophages press the angiogenic switch in breast cancer. Cancer Res. 2007;67(11):5064-6. Epub 2007/06/05. doi: 10.1158/0008-5472.CAN-07-0912. PubMed PMID: 17545580.
3. Singh S, Lee N, Bado I, Hamor C, Zhang L, Aguirre S, Hu J, Shen Y, Xu Y, Gao Y, Pedroza D, Zhao N, Chen S-H, Wan Y-W, Liu Z, Chang JT, Hollern D, Perou CM, Zhang XHF, Rosen JM. Synergy of chemotherapy and macrophage depletion leads to T cell memory activation and durable triple negative breast cancer regression. bioRxiv. 2021:2021.02.22.432300. doi: 10.1101/2021.02.22.432300.
4. Tekpli X, Lien T, Rossevold AH, Nebdal D, Borgen E, Ohnstad HO, Kyte JA, Vallon-Christersson J, Fongaard M, Due EU, Svartdal LG, Sveli MAT, Garred O, Osbreac, Frigessi A, Sahlberg KK, Sorlie T, Russnes HG, Naume B, Kristensen VN. An independent poor-prognosis subtype of breast cancer defined by a distinct tumor immune microenvironment. Nat Commun. 2019;10(1):5499. Epub 2019/12/05. doi: 10.1038/s41467-019-13329-5. PubMed PMID: 31796750; PMCID: PMC6890706.
5. Jerry DJ, Kittrell FS, Kuperwasser C, Laucirica R, Dickinson ES, Bonilla PJ, Butel JS, Medina D. A mammary-specific model demonstrates the role of the p53 tumor suppressor gene in tumor development. Oncogene. 2000;19(8):1052-8. Epub 2000/03/14. doi: 10.1038/sj.onc.1203270. PubMed PMID: 10713689.
6. Knezevic J, Pfefferle AD, Petrovic I, Greene SB, Perou CM, Rosen JM. Expression of miR-200c in claudin-low breast cancer alters stem cell functionality, enhances chemosensitivity and reduces metastatic potential. Oncogene. 2015;34(49):5997-6006. Epub 2015/03/10. doi: 10.1038/onc.2015.48. PubMed PMID: 25746005; PMCID: PMC4564359.
7. Hollern DP, Contreras CM, Dance-Barnes S, Silva GO, Pfefferle AD, Xiong J, Darr DB, Usary J, Mott KR, Perou CM. A mouse model featuring tissue-specific deletion of p53 and Brca1 gives rise to mammary tumors with genomic and transcriptomic similarities to human basal-like breast cancer. Breast Cancer Res Treat. 2019;174(1):143-55. Epub 2018/11/30. doi: 10.1007/s10549-018-5061-y. PubMed PMID: 30484104; PMCID: PMC6418066.
8. Kim IS, Gao Y, Welte T, Wang H, Liu J, Janghorban M, Sheng K, Niu Y, Goldstein A, Zhao N, Bado I, Lo HC, Toneff MJ, Nguyen T, Bu W, Jiang W, Arnold J, Gu F, He J, Jebakumar D, Walker K, Li Y, Mo Q, Westbrook TF, Zong C, Rao A, Sreekumar A, Rosen JM, Zhang XH. Immuno-subtyping of breast cancer reveals distinct myeloid cell profiles and immunotherapy resistance mechanisms. Nat Cell Biol. 2019;21(9):1113-26. Epub 2019/08/28. doi: 10.1038/s41556-019-0373-7. PubMed PMID: 31451770; PMCID: PMC6726554.
9. Hollern DP, Xu N, Thennavan A, Glodowski C, Garcia-Recio S, Mott KR, He X, Garay JP, Carey-Ewend K, Marron D, Ford J, Liu S, Vick SC, Martin M, Parker JS, Vincent BG, Serody JS, Perou CM. B Cells and T Follicular Helper Cells Mediate Response to Checkpoint Inhibitors in High Mutation Burden Mouse Models of Breast Cancer. Cell. 2019;179(5):1191-206 e21. Epub 2019/11/16. doi: 10.1016/j.cell.2019.10.028. PubMed PMID: 31730857; PMCID: PMC6911685.
10. Cabrita R, Lauss M, Sanna A, Donia M, Skaarup Larsen M, Mitra S, Johansson I, Phung B, Harbst K, Vallon-Christersson J, van Schoiack A, Lovgren K, Warren S, Jirstrom K, Olsson H, Pietras K, Ingvar C, Isaksson K, Schadendorf D, Schmidt H, Bastholt L, Carneiro A, Wargo JA, Svane IM, Jonsson G. Tertiary lymphoid structures improve immunotherapy and survival in melanoma. Nature. 2020;577(7791):561-5. Epub 2020/01/17. doi: 10.1038/s41586-019-1914-8. PubMed PMID: 31942071.
11. Khan KA, Ponce de Leon JL, Benguigui M, Xu P, Chow A, Cruz-Munoz W, Man S, Shaked Y, Kerbel RS. Immunostimulatory and anti-tumor metronomic cyclophosphamide regimens assessed in primary orthotopic and metastatic murine breast cancer. NPJ Breast Cancer. 2020;6:29. Epub 2020/07/25. doi: 10.1038/s41523-020-0171-1. PubMed PMID: 32704531; PMCID: PMC7371860.
12. Agudo J, Ruzo A, Park ES, Sweeney R, Kana V, Wu M, Zhao Y, Egli D, Merad M, Brown BD. GFP-specific CD8 T cells enable targeted cell depletion and visualization of T-cell interactions. Nat Biotechnol. 2015;33(12):1287-92. Epub 2015/11/03. doi: 10.1038/nbt.3386. PubMed PMID: 26524661; PMCID: PMC4675673.
13. Giustini N, Bernthal NM, Bukata SV, Singh AS. Tenosynovial giant cell tumor: case report of a patient effectively treated with pexidartinib (PLX3397) and review of the literature. Clin Sarcoma Res. 2018;8:14. Epub 2018/07/14. doi: 10.1186/s13569-018-0101-2. PubMed PMID: 30002809; PMCID: PMC6038319.
14. DeNardo DG, Brennan DJ, Rexhepaj E, Ruffell B, Shiao SL, Madden SF, Gallagher WM, Wadhwani N, Keil SD, Junaid SA, Rugo HS, Hwang ES, Jirstrom K, West BL, Coussens LM. Leukocyte complexity predicts

breast cancer survival and functionally regulates response to chemotherapy. Cancer Discov. 2011;1(1):54-67. Epub 2011/11/01. doi: 10.1158/2159-8274.CD-10-0028. PubMed PMID: 22039576; PMCID: PMC3203524.
15. Piawah S, Hyland C, Umetsu SE, Esserman LJ, Rugo HS, Chien AJ. A case report of vanishing bile duct syndrome after exposure to pexidartinib (PLX3397) and paclitaxel. NPJ Breast Cancer. 2019;5:17. Epub 2019/06/27. doi: 10.1038/s41523-019-0112-z. PubMed PMID: 31240240; PMCID: PMC6570645.
16. Gruosso T, Gigoux M, Manem VSK, Bertos N, Zuo D, Perlitch I, Saleh SMI, Zhao H, Souleimanova M, Johnson RM, Monette A, Ramos VM, Hallett MT, Stagg J, Lapointe R, Omeroglu A, Meterissian S, Buisseret L, Van den Eynden G, Salgado R, Guiot MC, Haibe-Kains B, Park M. Spatially distinct tumor immune microenvironments stratify triple-negative breast cancers. J Clin Invest. 2019;129(4):1785-800. Epub 2019/02/13. doi: 10.1172/JCI96313. PubMed PMID: 30753167; PMCID: PMC6436884.
17. Movahedi K, Laoui D, Gysemans C, Baeten M, Stange G, Van den Bossche J, Mack M, Pipeleers D, In't Veld P, De Baetselier P, Van Ginderachter JA. Different tumor microenvironments contain functionally distinct subsets of macrophages derived from Ly6C(high) monocytes. Cancer Res. 2010;70(14):5728-39. Epub 2010/06/24. doi: 10.1158/0008-5472.CAN-09-4672. PubMed PMID: 20570887.
18. Cao J, Spielmann M, Qiu X, Huang X, Ibrahim DM, Hill AJ, Zhang F, Mundlos S, Christiansen L, Steemers FJ, Trapnell C, Shendure J. The single-cell transcriptional landscape of mammalian organogenesis. Nature. 2019;566(7745):496-502. Epub 2019/02/23. doi: 10.1038/s41586-019-0969-x. PubMed PMID: 30787437; PMCID: PMC6434952.
19. La Manno G, Soldatov R, Zeisel A, Braun E, Hochgerner H, Petukhov V, Lidschreiber K, Kastriti ME, Lonnerberg P, Furlan A, Fan J, Borm LE, Liu Z, van Bruggen D, Guo J, He X, Barker R, Sundstrom E, Castelo-Branco G, Cramer P, Adameyko I, Linnarsson S, Kharchenko PV. RNA velocity of single cells. Nature. 2018;560(7719):494-8. Epub 2018/08/10. doi: 10.1038/s41586-018-0414-6. PubMed PMID: 30089906; PMCID: PMC6130801.
20. Lynn RC, Weber EW, Sotillo E, Gennert D, Xu P, Good Z, Anbunathan H, Lattin J, Jones R, Tieu V, Nagaraja S, Granja J, de Bourcy CFA, Majzner R, Satpathy AT, Quake SR, Monje M, Chang HY, Mackall CL. c-Jun overexpression in CAR T cells induces exhaustion resistance. Nature. 2019;576(7786):293-300. Epub 2019/12/06. doi: 10.1038/s41586-019-1805-z. PubMed PMID: 31802004; PMCID: PMC6944329.
21. Yang CY, Best JA, Knell J, Yang E, Sheridan AD, Jesionek AK, Li HS, Rivera RR, Lind KC, D'Cruz LM, Watowich SS, Murre C, Goldrath AW. The transcriptional regulators Id2 and Id3 control the formation of distinct memory CD8+ T cell subsets. Nat Immunol. 2011;12(12):1221-9. Epub 2011/11/08. doi: 10.1038/ni.2158. PubMed PMID: 22057289; PMCID: PMC3872000.
22. Wuerzberger-Davis SM, Chen Y, Yang DT, Kearns JD, Bates PW, Lynch C, Ladell NC, Yu M, Podd A, Zeng H, Huang TT, Wen R, Hoffmann A, Wang D, Miyamoto S. Nuclear export of the NF-kappaB inhibitor IkappaBalpha is required for proper B cell and secondary lymphoid tissue formation. Immunity. 2011;34(2):188-200. Epub 2011/02/22. doi: 10.1016/j.immuni.2011.01.014. PubMed PMID: 21333553; PMCID: PMC3111750.
23. Menares E, Galvez-Cancino F, Caceres-Morgado P, Ghorani E, Lopez E, Diaz X, Saavedra-Almarza J, Figueroa DA, Roa E, Quezada SA, Lladser A. Tissue-resident memory CD8(+) T cells amplify anti-tumor immunity by triggering antigen spreading through dendritic cells. Nat Commun. 2019;10(1):4401. Epub 2019/09/29. doi: 10.1038/s41467-019-12319-x. PubMed PMID: 31562311; PMCID: PMC6765014.
24. Yost KE, Satpathy AT, Wells DK, Qi Y, Wang C, Kageyama R, McNamara KL, Granja JM, Sarin KY, Brown RA, Gupta RK, Curtis C, Bucktrout SL, Davis MM, Chang ALS, Chang HY. Clonal replacement of tumor-specific T cells following PD-1 blockade. Nat Med. 2019;25(8):1251-9. Epub 2019/07/31. doi: 10.1038/s41591-019-0522-3. PubMed PMID: 31359002; PMCID: PMC6689255.
25. Cano-Gamez E, Soskic B, Roumeliotis TI, So E, Smyth DJ, Baldrighi M, Wille D, Nakic N, Esparza-Gordillo J, Larminie CGC, Bronson PG, Tough DF, Rowan WC, Choudhary JS, Trynka G. Single-cell transcriptomics identifies an effectorness gradient shaping the response of CD4(+) T cells to cytokines. Nat Commun. 2020;11(1):1801. Epub 2020/04/15. doi: 10.1038/s41467-020-15543-y. PubMed PMID: 32286271; PMCID: PMC7156481.
26. Jabara HH, Weng Y, Sannikova T, Geha RS. TRAF2 and TRAF3 independently mediate Ig class switching driven by CD40. Int Immunol. 2009;21(4):477-88. Epub 2009/02/21. doi: 10.1093/intimm/dxp013. PubMed PMID: 19228877; PMCID: PMC2721683.
27. Tang H, Zhu M, Qiao J, Fu YX. Lymphotoxin signalling in tertiary lymphoid structures and immunotherapy. Cell Mol Immunol. 2017;14(10):809-18. Epub 2017/04/18. doi: 10.1038/cmi.2017.13. PubMed PMID: 28413217; PMCID: PMC5649108.
28. Cortes J, Cescon DW, Rugo HS, Nowecki Z, Im SA, Yusof MM, Gallardo C, Lipatov O, Barrios CH, Holgado E, Iwata H, Masuda N, Otero MT, Gokmen E, Loi S, Guo Z, Zhao J, Aktan G, Karantza V, Schmid P,

Investigators K-. Pembrolizumab plus chemotherapy versus placebo plus chemotherapy for previously untreated locally recurrent inoperable or metastatic triple-negative breast cancer (KEYNOTE-355): a randomised, placebo-controlled, double-blind, phase 3 clinical trial. Lancet. 2020;396(10265):1817-28. Epub 2020/12/07. doi: 10.1016/S0140-6736(20)32531-9. PubMed PMID: 33278935.
29. Zhang L, Li Z, Skrzypczynska KM, Fang Q, Zhang W, O'Brien SA, He Y, Wang L, Zhang Q, Kim A, Gao R, Orf J, Wang T, Sawant D, Kang J, Bhatt D, Lu D, Li CM, Rapaport AS, Perez K, Ye Y, Wang S, Hu X, Ren X, Ouyang W, Shen Z, Egen JG, Zhang Z, Yu X. Single-Cell Analyses Inform Mechanisms of Myeloid-Targeted Therapies in Colon Cancer. Cell. 2020;181(2):442-59 e29. Epub 2020/04/18. doi: 10.1016/j.cell.2020.03.048. PubMed PMID: 32302573.
30. Bonekamp NA, Peter B, Hillen HS, Felser A, Bergbrede T, Choidas A, Horn M, Unger A, Di Lucrezia R, Atanassov I, Li X, Koch U, Menninger S, Boros J, Habenberger P, Giavalisco P, Cramer P, Denzel MS, Nussbaumer P, Klebl B, Falkenberg M, Gustafsson CM, Larsson NG. Small-molecule inhibitors of human mitochondrial DNA transcription. Nature. 2020. Epub 2020/12/18. doi: 10.1038/s41586-020-03048-z. PubMed PMID: 33328633.
31. Whittle JR, Vaillant F, Surgenor E, Policheni AN, Giner G, Capaldo BD, Chen HR, Liu HK, Dekkers JF, Sachs N, Clevers H, Fellowes A, Green T, Xu H, Fox SB, Herold MJ, Smyth GK, Gray DHD, Visvader JE, Lindeman GJ. Dual Targeting of CDK4/6 and BCL2 Pathways Augments Tumor Response in Estrogen Receptor-Positive Breast Cancer. Clin Cancer Res. 2020;26(15):4120-34. Epub 2020/04/05. doi: 10.1158/1078-0432.CCR-19-1872. PubMed PMID: 32245900.
32. Stuart T, Butler A, Hoffman P, Hafemeister C, Papalexi E, Mauck WM, 3rd, Hao Y, Stoeckius M, Smibert P, Satija R. Comprehensive Integration of Single-Cell Data. Cell. 2019;177(7):1888-902 e21. Epub 2019/06/11. doi: 10.1016/j.cell.2019.05.031. PubMed PMID: 31178118; PMCID: PMC6687398.
33. Aran D, Looney AP, Liu L, Wu E, Fong V, Hsu A, Chak S, Naikawadi RP, Wolters PJ, Abate AR, Butte AJ, Bhattacharya M. Reference-based analysis of lung single-cell sequencing reveals a transitional profibrotic macrophage. Nat Immunol. 2019;20(2):163-72. Epub 2019/01/16. doi: 10.1038/s41590-018-0276-y. PubMed PMID: 30643263; PMCID: PMC6340744.
34. Ramilowski JA, Goldberg T, Harshbarger J, Kloppmann E, Lizio M, Satagopam VP, Itoh M, Kawaji H, Carninci P, Rost B, Forrest AR. A draft network of ligand-receptor-mediated multicellular signalling in human. Nat Commun. 2015;6:7866. Epub 2015/07/23. doi: 10.1038/ncomms8866. PubMed PMID: 26198319; PMCID: PMC4525178.
35. Vento-Tormo R, Efremova M, Botting RA, Turco MY, Vento-Tormo M, Meyer KB, Park JE, Stephenson E, Polanski K, Goncalves A, Gardner L, Holmqvist S, Henriksson J, Zou A, Sharkey AM, Millar B, Innes B, Wood L, Wilbrey-Clark A, Payne RP, Ivarsson MA, Lisgo S, Filby A, Rowitch DH, Bulmer JN, Wright GJ, Stubbington MJT, Haniffa M, Moffett A, Teichmann SA. Single-cell reconstruction of the early maternal-fetal interface in humans. Nature. 2018;563(7731):347-53. Epub 2018/11/16. doi: 10.1038/s41586-018-0698-6. PubMed PMID: 30429548.
36. Horak CE, Pusztai L, Xing G, Trifan OC, Saura C, Tseng LM, Chan S, Welcher R, Liu D. Biomarker analysis of neoadjuvant doxorubicin/cyclophosphamide followed by ixabepilone or Paclitaxel in early-stage breast cancer. Clin Cancer Res. 2013;19(6):1587-95. Epub 2013/01/24. doi: 10.1158/1078-0432.CCR-12-1359. PubMed PMID: 23340299.
37. Park YH, Lal S, Lee JE, Choi YL, Wen J, Ram S, Ding Y, Lee SH, Powell E, Lee SK, Yu JH, Ching KA, Nam JY, Kim SW, Nam SJ, Kim JY, Cho SY, Park S, Kim J, Hwang S, Kim YJ, Bonato V, Fernandez D, Deng S, Wang S, Shin H, Kang ES, Park WY, Rejto PA, Bienkowska J, Kan Z. Chemotherapy induces dynamic immune responses in breast cancers that impact treatment outcome. Nat Commun. 2020;11(1):6175. Epub 2020/12/04. doi: 10.1038/s41467-020-19933-0. PubMed PMID: 33268821; PMCID: PMC7710739 D., Deng S., Wang S., Rejto P., Bienkowska J. and Kan Z. were employees of Pfizer Inc. at the time the work was performed. All other authors declare no potential conflicts of interest.
38. Chen X, Chang JT. Planning bioinformatics workflows using an expert system. Bioinformatics. 2017;33(8):1210-5. Epub 2017/01/06. doi: 10.1093/bioinformatics/btw817. PubMed PMID: 28052928; PMCID: PMC5860174.
39. Dobin A, Davis CA, Schlesinger F, Drenkow J, Zaleski C, Jha S, Batut P, Chaisson M, Gingeras TR. STAR: ultrafast universal RNA-seq aligner. Bioinformatics. 2013;29(1):15-21. Epub 2012/10/30. doi: 10.1093/bioinformatics/bts635. PubMed PMID: 23104886; PMCID: PMC3530905.
40. Anders S, Pyl PT, Huber W. HTSeq--a Python framework to work with high-throughput sequencing data. Bioinformatics. 2015;31(2):166-9. Epub 2014/09/28. doi: 10.1093/bioinformatics/btu638. PubMed PMID: 25260700; PMCID: PMC4287950.
41. Subramanian A, Tamayo P, Mootha VK, Mukherjee S, Ebert BL, Gillette MA, Paulovich A, Pomeroy SL,

Golub TR, Lander ES, Mesirov JP. Gene set enrichment analysis: a knowledge-based approach for interpreting genome-wide expression profiles. Proc Natl Acad Sci U S A. 2005;102(43):15545-50. Epub 2005/10/04. doi: 10.1073/pnas.0506580102. PubMed PMID: 16199517; PMCID: PMC1239896.
42. Liberzon A, Subramanian A, Pinchback R, Thorvaldsdottir H, Tamayo P, Mesirov JP. Molecular signatures database (MSigDB) 3.0. Bioinformatics. 2011;27(12):1739-40. Epub 2011/05/07. doi: 10.1093/bioinformatics/btr260. PubMed PMID: 21546393; PMCID: PMC3106198.

Main Figure Legends

Figure 1-
p53 -/- syngeneic TNBC GEM recapitulate human TNBC subtypes and respond to low dose immunostimulatory chemotherapy treatment

a, Heatmap for pathways enriched in p53-/- tumor models. **b,** Cibersort analysis for immune cells on p53 -/- tumor models**. c,** Principal component analysis (PCA) on p53 -/- tumor models. **d,** Single agent CTX treatment led to a reduced tumor burden in Balb/c mice as compared to NSG mice. Data are shown as mean S.E.M, n = 10 per group except NSG PBS, n = 5. Multiple unpaired t tests were used to determine significance**. e**, Antibody depletion of CD4+ T Cells leads to a significant decrease in response to CTX and increased tumor volumes while differences in response due to depletion of CD8+ T Cells neared statistical significance at day 17, p = 0.06 n = 5-7 mice per group. Multiple unpaired t tests were used to determine significance. **f,** Treatment schema for combination therapy using low-dose Cyclophosphamide (CTX) and a CSF1R inhibitor
Pexidartinib (PXB**). g,h,i** Improved survival in mouse tumor models after combination treatment. Treatment was stopped at day 30**. j,k,l**, Combining low-dose CTX with a Csf1r inhibitor (PXB) lead to a reduction in tumor burden in T12 and 2151R p53-/- mouse tumors and stasis in T11, n = 7-10 mice per group. Survival benefit was assessed by Kaplan-Meier curves using the log-rank (Mantel-Cox) test. Dotted line marks point of treatment cessation.

Figure 2- Imaging Mass Cytometry and Single cell RNA sequencing show that combination treatment can lead to an expansion of CD8+/CD4+ T cells and B cells in responsive T12 tumors. a, Imaging mass cytometry analysis of the tumor immune microenvironment in T12 tumors before and after treatment. Representative images overlaid with 7 markers (F480, Ly6C, Ly6G, CD11b, CD4, CD8a, B220) for each treatment group. **b, c** Map using *t*-distributed stochastic neighbour embedding(*t*-SNE) of immune cells from high dimensional images of T12 tumors from treatment groups-PBS, PXB, CTX, CTX + PXB, n = 3 mice per group. **d,** Neighborhood analysis of T12 tumors in which the color of the squares indicates significant pairwise interactions or avoidance between PhenoGraph defined cellular metaclusters. Highlighted interactions include CD8+/CD4+ T cells (clusters 1-7), B220+ B cells(cluster-14) and CD11C+ CD86+ Dendritic cells (cluster 15). **e,** UMAP plot showing CD45+ immune cell clusters before and after treatment. **f,** UMAP plot showing CD45+ immune cells split by treatment group. **g,** Quantification of main immune cell clusters in 4 treatment groups.

Figure 3-Single cell RNA sequencing and IMC reveal phenotypically similar (F480+) but transcriptomically distinct TAMs in responsive(T12) and non-responsive(T11) tumors. a, UMAP plot showing CD68+ Myeloid cells sub-clysters including LY6C2+ Monocytes, IRF7+ TAMS, ACP5+ TAMS and S100A4+TAMS from untreated T12 and T11 tumors (2 per group)**. b,** Quantification of TAM sub-clusters in untreated T12 and T11 tumors.**c,** Projection of CD68+ Myeloid cells along a pseudotime trajectory with the root point starting at Ly6c2+ monocytes showing that T12 and T11 TAMs follow distinct development trajectories. **d,** Plot showing differentially expressed genes between T12 TAMs and T11 TAMs (log2fold change>1.5, $p < 0.05$). **e,** Quantification of CSF1R expression in T12 and T11 TAMS. P values > 0.05 were considered significant and calculated using Wilcoxan Rank Sum Test. **f,** Enrichment of select activation and metabolism related pathways in T12 and T11 CD68+ Myeloid cells using GSEA. **g,** Representative IMC images of T12 and T11 tumors after combination therapy highlighting the

spatial localization of CD8+/CD4+ T cells and B cells with respect to proliferating Ki67+ cells and F480+ TAMs.

Figure 4-Combination therapy treated T12 tumors are infiltrated by polyclonally expanded, less differentiated, exhaustion-resistant CD8+ T cells. a, UMAP plot showing CD8+ T Cell clusters of the 4 treatment groups and split by sample type. Clusters were annotated using the Immgen database (5), SingleR(Data not shown) and using known markers. **b,** Quantification of CD8+ T cell subsets in different treatment groups. **c,** Monocle 3 pseudotime plot of CD8+ T cells from all 4 treatment groups in T12 tumors. **d,** Gene expression of exhaustion and activation/longevity related markers in CD8+ T Cell clusters across pseudotime, split by treatment group. **e,** Clonal frequency of CD8+ T cells in all 4 treatment groups and chord diagrams representing unique V-J region pairings in CD8+ T cells in T12 tumors before and after treatment. h, Schema for T12 rechallenge experiments and treatment. **f,** Quantification of mice that completely or partially (tumor volume < 50 % of control tumors) rejected T12 mammary tumors injected into the contralateral mammary gland of previously treated T12 tumor bearing mice, n = 10. **g,** Treatment schema depicting treatment for mice bearing T12 lung metastasis. **H,** Representative images and quantification of surface metastatic lung nodules in all 4 treatment groups-PBS, PXB, CTX, CTX+PXB, n= 5-6 animals per group, $p < 0.05$).

Figure 5- CD4 T cell and B cell play an important role in mediating long term tumor regression. a, UMAP plot showing CD4+ T Cell clusters in the 4 treatment groups.Clusters were annotated using the Immgen database (5), SingleR(Data not shown) and using known markers. b, Quantification of CD4+ T cell subsets in different treatment groups. c, Monocle 3 pseudotime plot of CD4+ T cells from all 4 treatment groups in T12 tumors arising from a common naïve progenitor population, d, Heatmap showing highly expressed genes per CD4+ T cell sub-cluster. e, Violin plots showing the expression of select memory, activation and exhaustion markers in CD4+ T cell sub-clusters. f, Select ligand-receptor pairs involved in CD4+ T cell and CD19+ B cell signaling. P values < 0.01 were considered significant(See Methods). List of significant ligand receptor analysis between CD4 T cells and CD19+ B cells, CD68+ Myeloid Cells and ITGAX+ Dendritic cells is available in the supplementary materials

Figure 6- **Activated B cells expand after combination immunotherapy and are the main antigen presenting cells to CD4+ T memory cells with tertiary lymphoid structures.** **a,** UMAP plot showing CD19+ B Cell clusters of the 4 treatment groups and split by sample type. Clusters were annotated using the Immgen database (5), SingleR(Data not shown) and using known markers. **b,** Monocle 3 pseudotime plot of CD19+ B cells from all 4 treatment groups in T12 tumors arising from a common B cell population **c,** Quantification of CD19+ B cell subsets in different treatment groups. **d,** Pathway analysis showing select enriched biological process pathways in activated CD86+ B cells that expand after combination treatment. **e,** Imaging Mass Cytometry analysis of TLS observed 30 days post-treatment in long-term responder mice bearing T12 tumors. Representative image overlaid with 4 markers (F480, CD8A, B220, CD4, CD44, CD11C, CD86) in the site of completely regressed primary tumors in combination treated mice 30 days post-treatment. **e,f,** Neighborhood analysis of tertiary lymphois structures in which the color of the squares indicates significant pairwise interactions(Red),avoidance(Blue) or a complete lack of interactions(White) between PhenoGraph defined cellular metaclusters. Highlighted interactions include CD4+/CD44+ memory T cells cells (clusters 4-5) with B220+/CD86+ B cells(cluster 9) and CD11C+ Dendritic cells (cluster 15)

Figure 7-Activated B cell signatures correlate with pCR in multiple datasets of TNBC patients undergoing neoadjuvant chemotherapy. a, Expression of canonical B cell markers CD19 and CD20 in bulk RNA sequencing data from patients across all subtypes of breast cancer pre NAC(GSE41988). **b,** Expression of canonical B cell markers CD19 and CD20 in triple negative breast cancer . **c,** Multivariate analysis of patient response to neoadjuvant chemotherapy(Adriamycin+ CTX) using known B cell markers and a signature for CD86+ activated B cells. **d,** Multivariate analysis of patient response to neoadjuvant chemotherapy(Adriamycin+ CTX) using known B cell markers and a signature with genes upregulated in T11 and T12 TAMs.

Supplemental Figure Legends

Supplemental Figure 1 p53 -/- syngeneic TNBC GEM recapitulate human TNBC subtypes and respond to low dose immunostimulatory chemotherapy treatment .
a, Treatment response using standard of care drugs on T11 mammary tumors. **b,** Immunohistochemistry for F4/80+ TAMs and CD8+ T Cells on p53-/- tumor models. **c,** T cell gating scheme. **d,** Myeloid cell gating scheme. **e,** Co-culture of GFP+ T12 tumor cells and GFP targeting T cells with or without Phosphoramide Mustard (PM). Each treatment was performed in triplicates and repeated twice. **f,** Flow cytometry analysis of CD8+ and CD4+ T cells before and after low-dose CTX treatment, n =
6-7 mice per group. **g,** Quantification of TAMs upon antibody depletion of CD4+ T cells after treatment. **h,** Quantification of CD8+ T cells after CD4+ T cell depletion after treatment. **i,j,** Quantification of CD8+ T memory cell subsets before and after treatment, n = 4-5 mice per group. Unpaired t-test was used to determine significance. **k,l,,** Reduced tumor volume and improved survival in T12 mammary tumor bearing mice after treatment with CTX and 3.3X lower PXB (75 ppm).

Supplemental Figure 2- Imaging Mass Cytometry and Single cell RNA sequencing show that combination treatment can lead to an expansion of CD8+/CD4+ T cells and B cells in responsive(T11) and non responsive(T11) tumor models. a, . a, Imaging mass cytometry analysis of the tumor immune microenvironment in T11 tumors before and after treatment. Representative images overlaid with 7 markers (F480, Ly6C, Ly6G, CD11b, CD4, CD8a, B220) for each treatment group. **b,c,** Map using *t*-distributed stochastic neighbour embedding(*t*-SNE) of immune cells from high dimensional images of non-responsive T11 tumors from treatment groups-PBS, PXB, CTX, CTX + PXB, n = 3 mice per group. **d,** Neighborhood analysis of T11 tumors in which the color of the squares indicates significant pairwise interactions or avoidance between PhenoGraph defined cellular metaclusters. Highlighted interactions include CD8+/CD4+ T cells (clusters 1-7), B220+ B cells(cluster-15) and CD11C+ CD86+ Dendritic cells (cluster 16). **c,** Flow cytometry quantification of T12 and T11 tumor associated macrophages after combination therapy. **f,** Gene expression heatmap for CD45+ immune cells before and after treatment for all treatment groups. **g,** Feature plots showing the expression levels of murine immune cell marker genes (CD3e, CD4, Cd8a, CD19, CD68, S100A8, ITGAX in all 4 treatment groups. **h,** GOBP analysis of S100A8+ neutrophils that increase in T12 tumors after single agent PXB treatment. **i,** IHC showing elevated pMAPK signalling in T11 tumors pre-treatment.**j,** Integrative Genomics Viewer(IGV) image showing G12V activating mutation in T11 tumor and T11 cell line(Highlighted in neon green)

Supplemental Figure 3-Single cell RNA sequencing and IMC reveal phenotypically similar (F480+) but transcriptomically distinct TAMs in responsive(T12) and non-responsive(T11) tumors. a, Heatmap showing top 10 upregulated genes per TAM sub-cluster for T12 and T11. **b,** PCA progression using Velocyto showing the distinct differentiation trajectories followed by T12 an dT11 TAMs arising from a common progenitor monocyte population. **c,** Quantification of additional TAM marker genes.**d,** Heatmap representing top upregulated and downregulated immune and metabolic pathways in T12 TAMs. **e,** qPCR analysis of T12, T11 and 2151R

tumors using select genes related to oxidative phosphorylation(n – 3 per model, p value calculated using multiple T tests**. f,** In-vitro co-culture assay with sorted F480+ TAMs from T12 and T11 tumor models with GFP targeting JEDI T cells and GFP+ T12 tumor cells. Each condition was run in triplicate and the impact of TAMs on T12 tumor cell proliferation was measured by Ki67 staining.

Supplemental Figure 4-Combination therapy treated T12 tumors are infiltrated by polyclonally expanded, less differentiated, exhaustion-resistant CD8+ memory T cells. a, Gene expression heatmap top genes for each CD8+ T cell sub-cluster **b,** V(D)J analysis of CD8+ T cells for all 4 treatment groups showing polyclonal expansion of CD8+ T cells after combination treatment.**c,** Feature plots showing the expression of select memory/exhaustion/activation markers in CD8+ T cells. **d,** Schema for T12 rechallenge experiments and treatment. **e** Quantification of mice that completely or partially (tumor volume < 50 % of control tumors) rejected T12 mammary tumors injected into the contralateral mammary gland of previously treated T12 tumor bearing mice, n = 10.

Supplemental Figure 5- CD4 T cell and B cell play an important role in mediating long term tumor regression. a, Clonal frequency of CD4+ T cells in all 4 treatment groups and chord diagrams representing unique V-J region pairings in CD4+ T cells in T12 tumors before and after treatment. **b,** PCA progression using Velocyto showing the distinct differentiation trajectories followed by CD4+ T cell sub-clusters arising from a CD4+ T naïve population. **c,** Feature plots showing the expression of select memory/exhaustion/activation markers in CD4+ T cells across all 4 treatment groups.**d,** Violin plots showing expression of additional T cell memory, exhaustion and anti-apoptosis markers.

Supplemental Figure 6- Activated B cells expand after combination immunotherapy and are the main antigen presenting cells to CD4+ T memory cells with tertiary lymphoid structures.
a, Heatmap showing highly expressed genes in every B cell sub-cluster**.** b H&E and IHC images of TLS using T cell (CD4+ or CD8+) and B cell (CD19+) markers. b, Representative imaging mass cytometry images as well as single channel images depicting the localization of HEV marker Endomucins with B220+ B cells and CD4+ T cells withing TLS. **e,** Quantification of TLS in all 4 treatment groups($p < 0.05$). **f,** Quantification of Phenograph defined cell sub-clusters with the TLS.

Supplemental Figure 7. Activated B cell signatures correlate with pCR in multiple datasets of TNBC patients undergoing neoadjuvant chemotherapy. a, Multivariate analysis of patient response to neoadjuvant chemotherapy(Adriamycin+ CTX) using known B cell

markers and a signature for total infiltrating lymphocytes(TIL). **b,** Multivariate analysis of patient response to neoadjuvant chemotherapy(Adriamycin+ CTX) using known the activated CD86+ B cell signature and CD19/CD20 which are known B cell markers. **c,** Association of CD19 and CD20 with response to neoadjuvant chemotherapy.

.

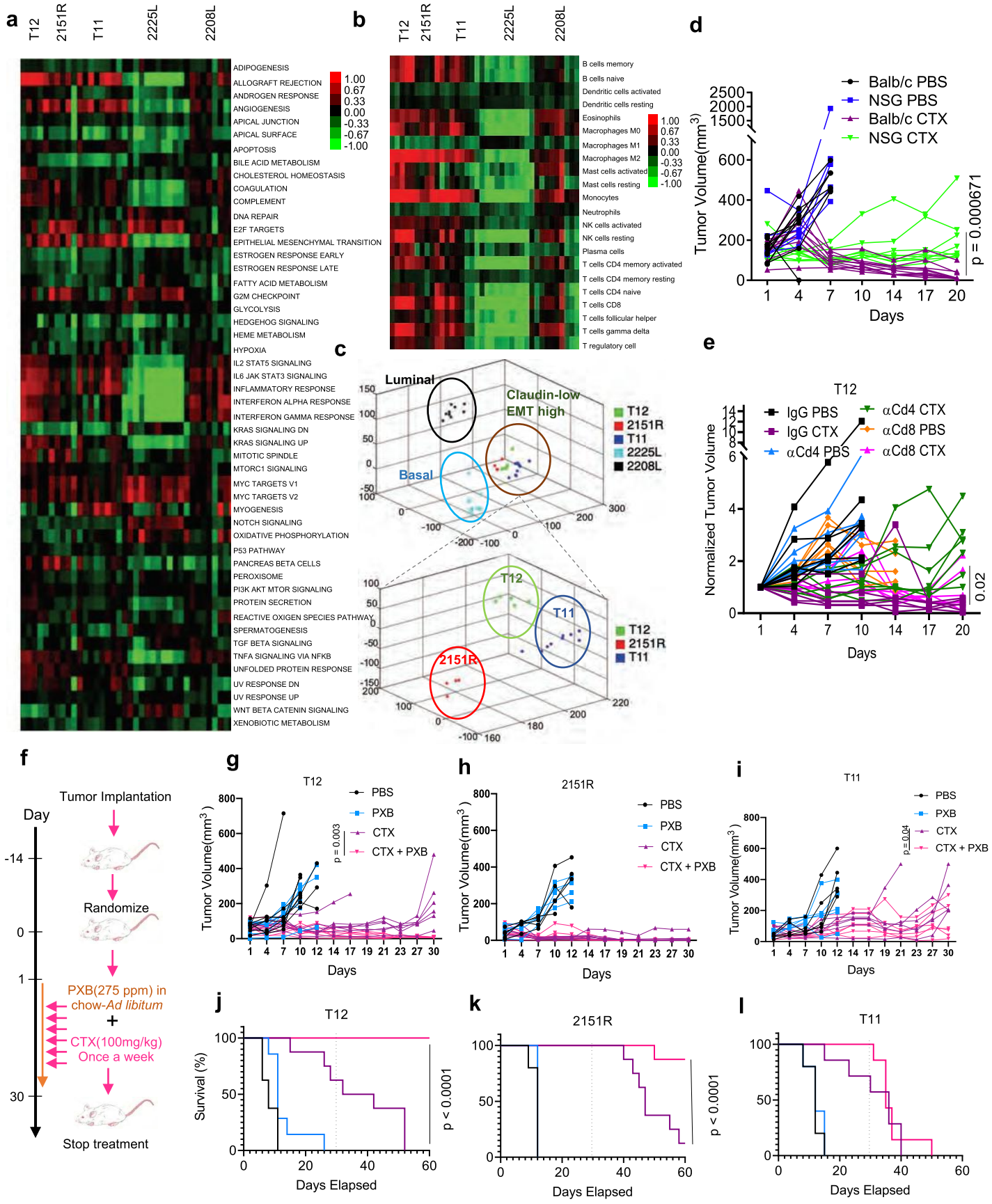

Figure 1, Singh et al.

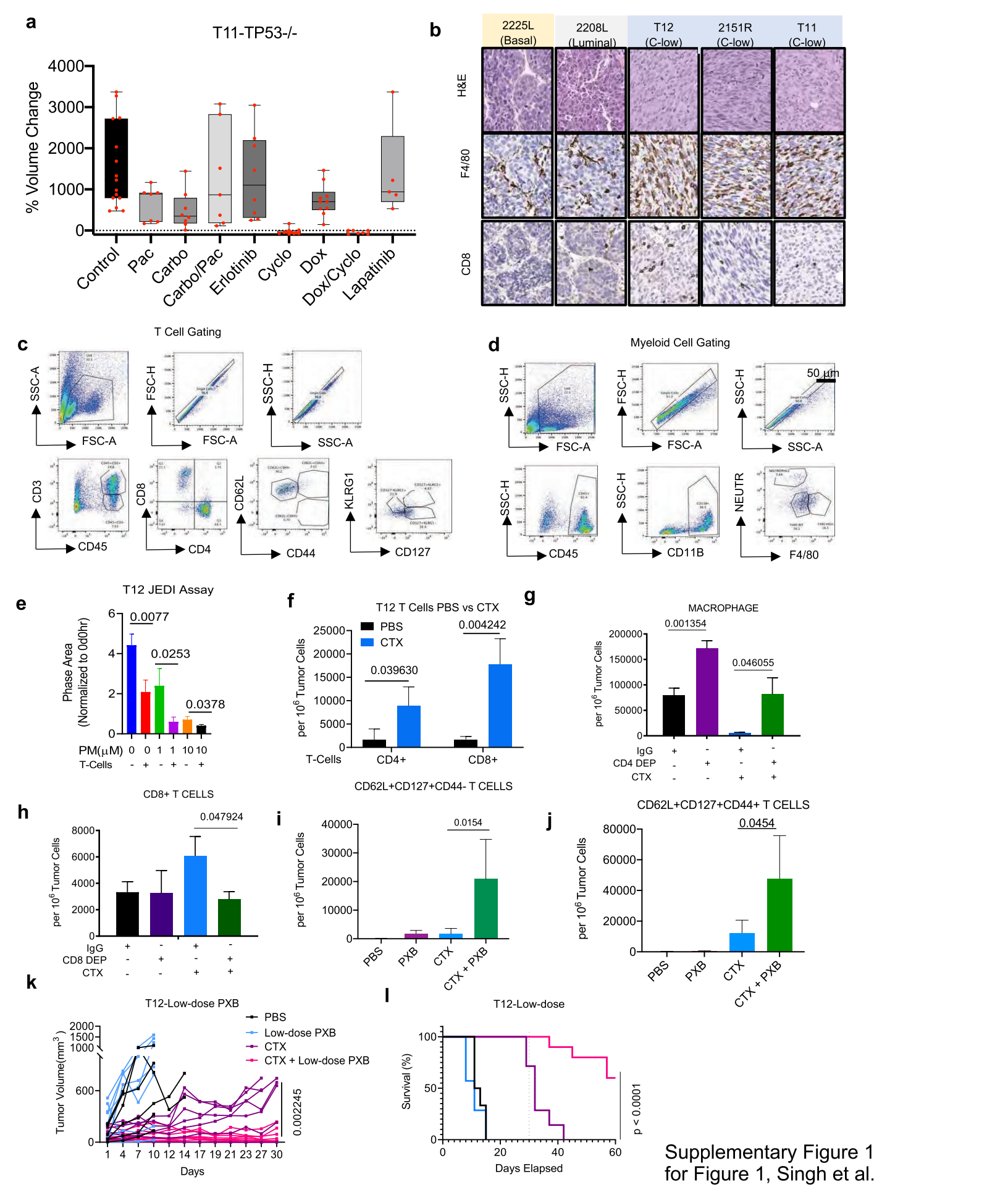

Supplementary Figure 1
for Figure 1, Singh et al.

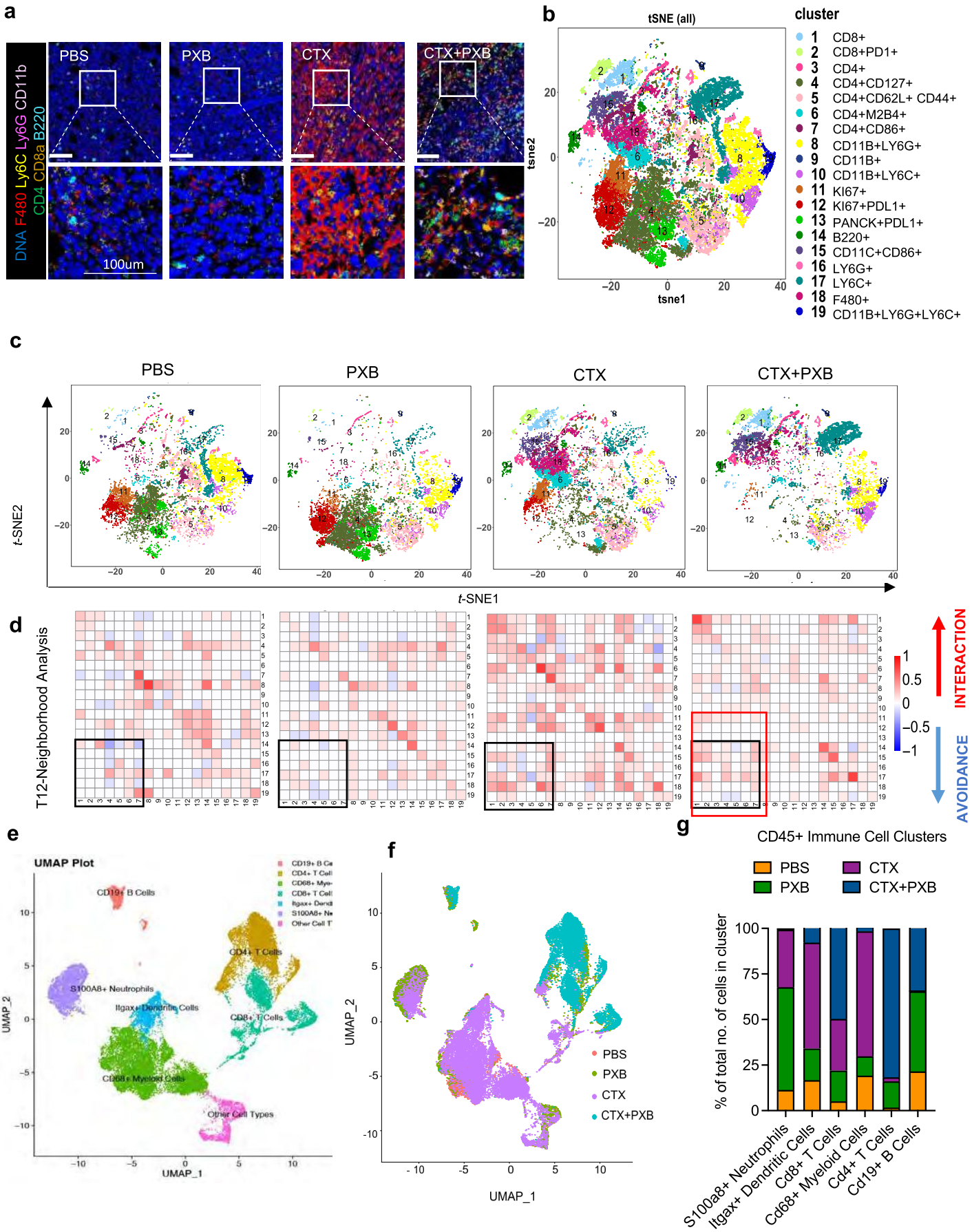

Figure 2, Singh et al.

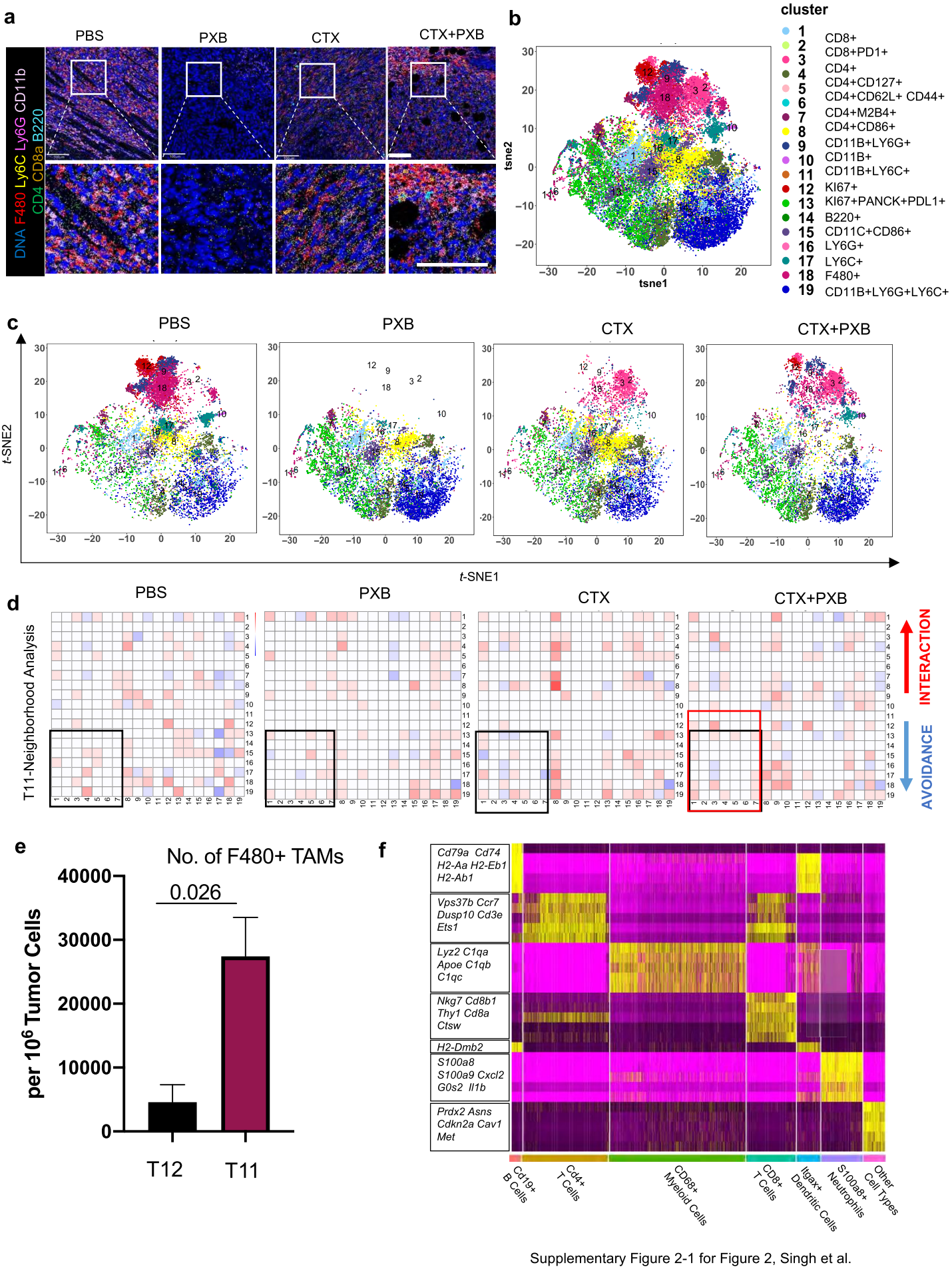

Supplementary Figure 2-1 for Figure 2, Singh et al.

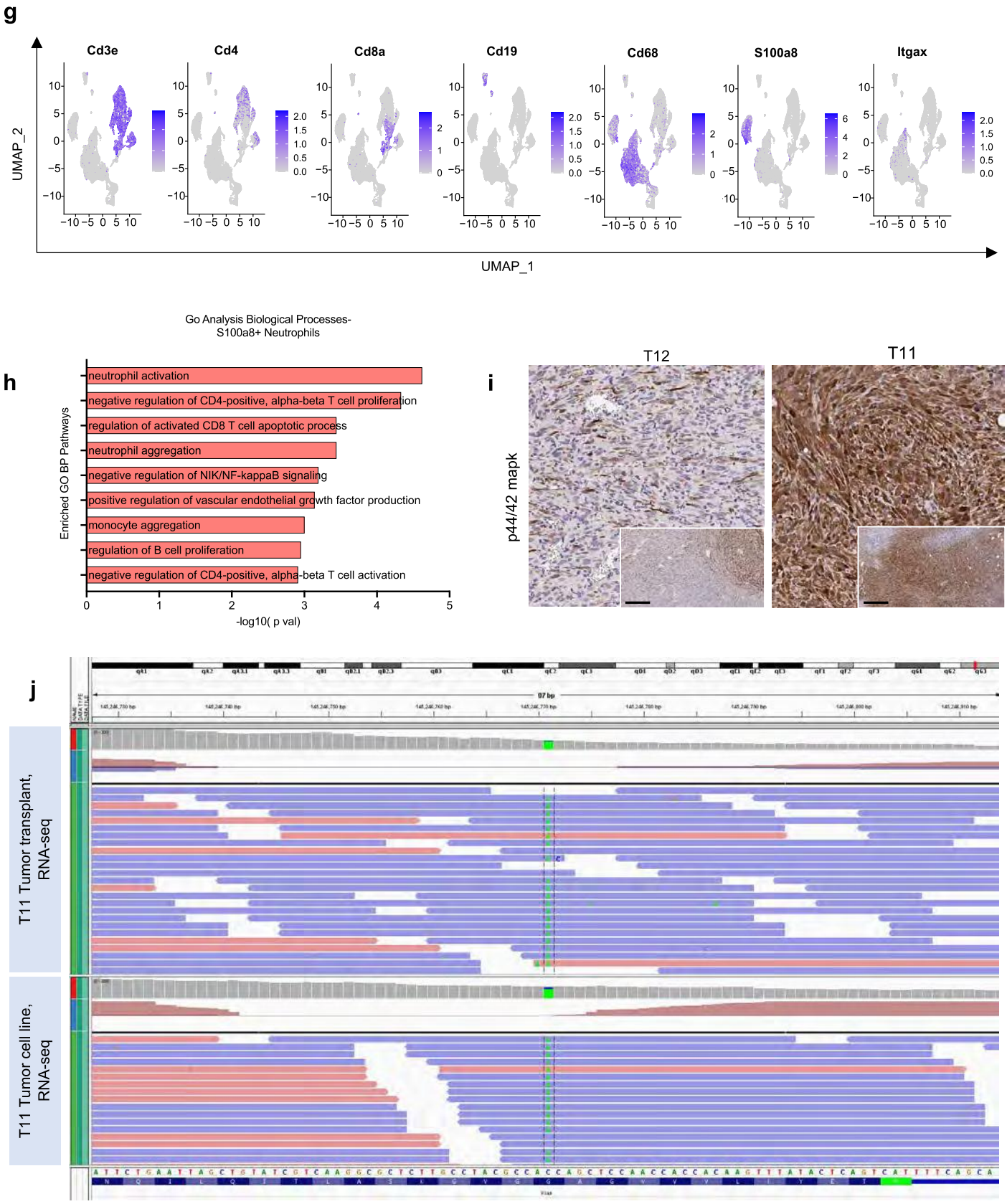

Supplementary Figure 2 -2 for Figure 2, Singh et al.

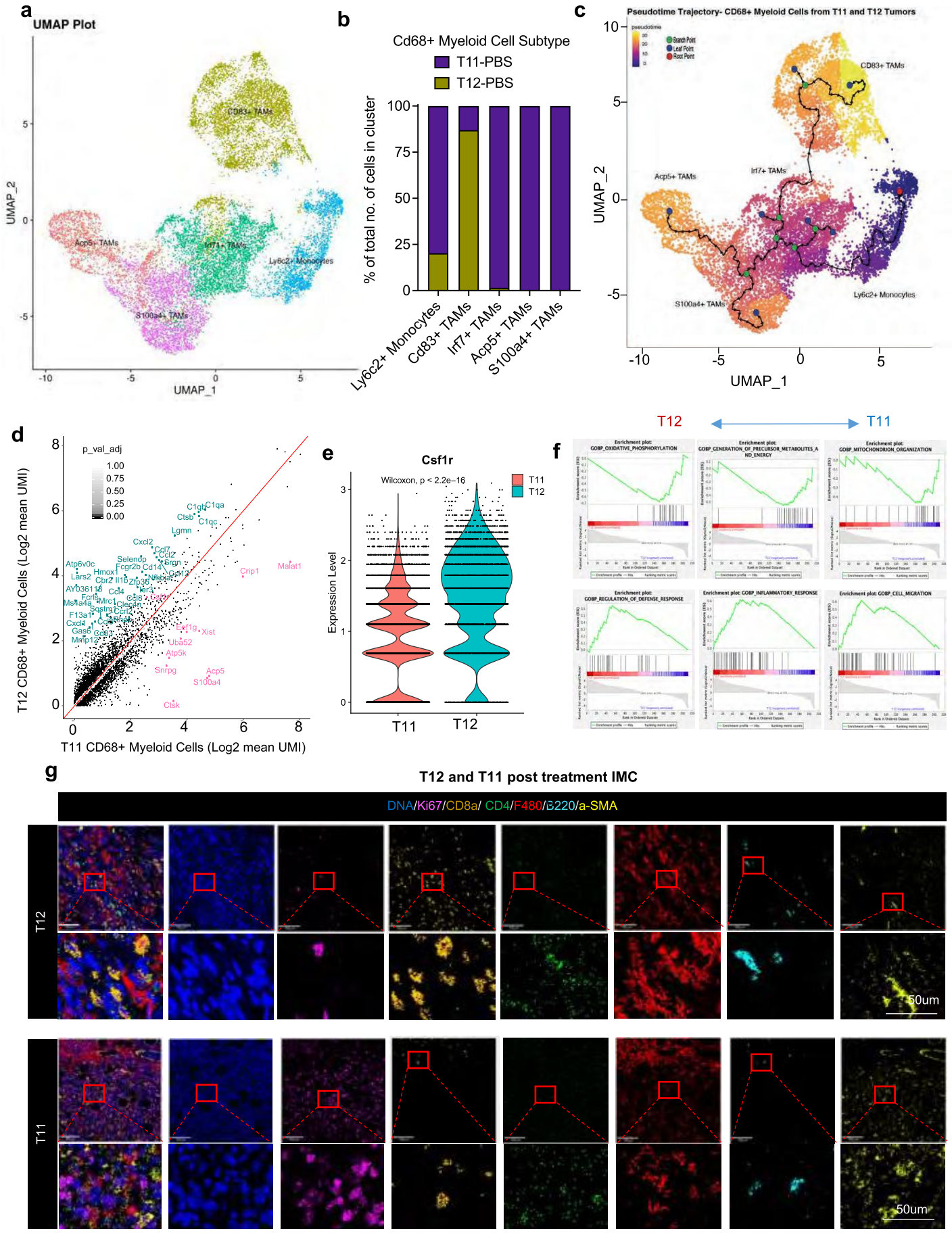

Figure 3, Singh et al.

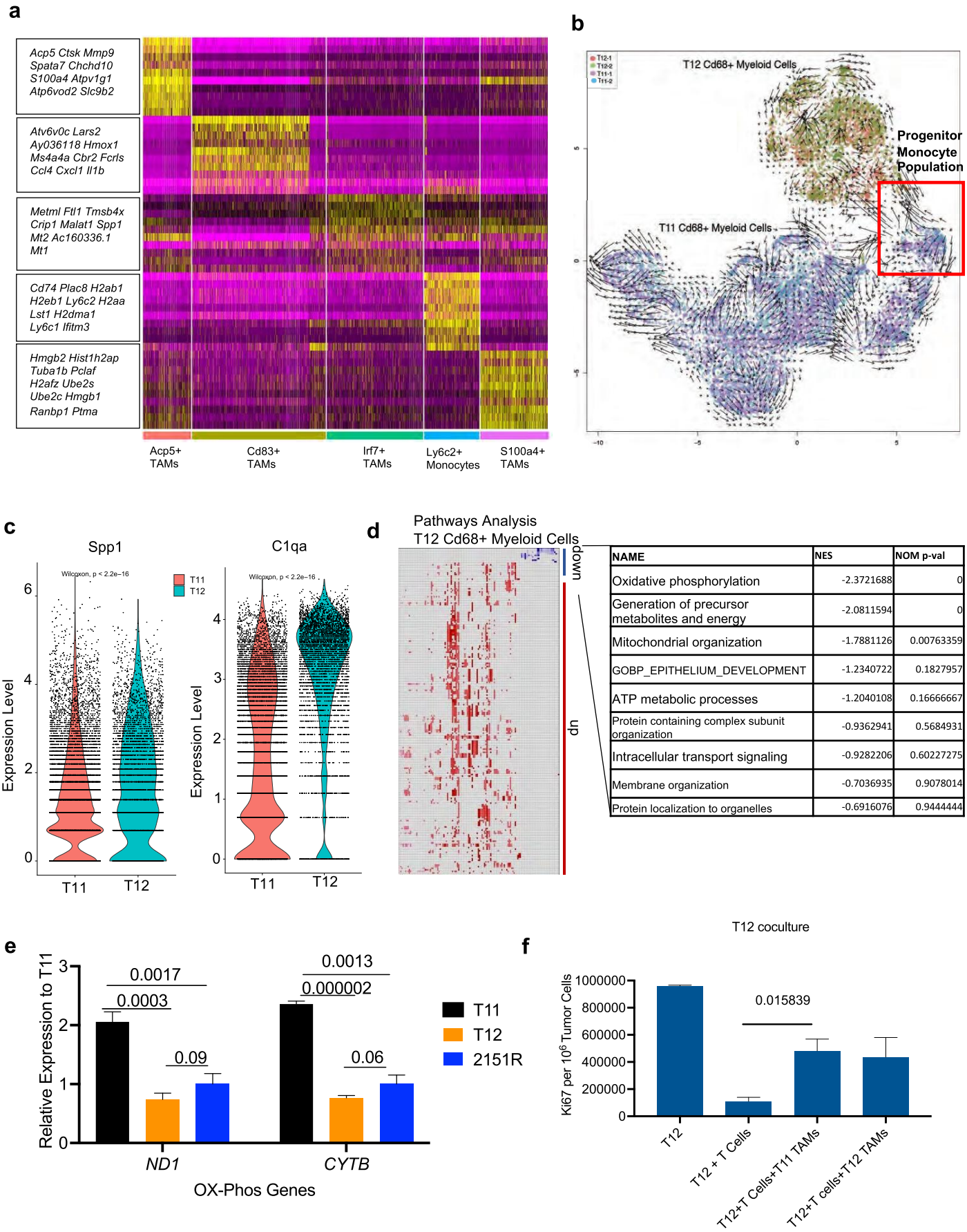

NAME	NES	NOM p-val
Oxidative phosphorylation	-2.3721688	0
Generation of precursor metabolites and energy	-2.0811594	0
Mitochondrial organization	-1.7881126	0.00763359
GOBP_EPITHELIUM_DEVELOPMENT	-1.2340722	0.1827957
ATP metabolic processes	-1.2040108	0.16666667
Protein containing complex subunit organization	-0.9362941	0.5684931
Intracellular transport signaling	-0.9282206	0.60227275
Membrane organization	-0.7036935	0.9078014
Protein localization to organelles	-0.6916076	0.9444444

Supplementary Figure 3 for Figure 3, Singh et al.

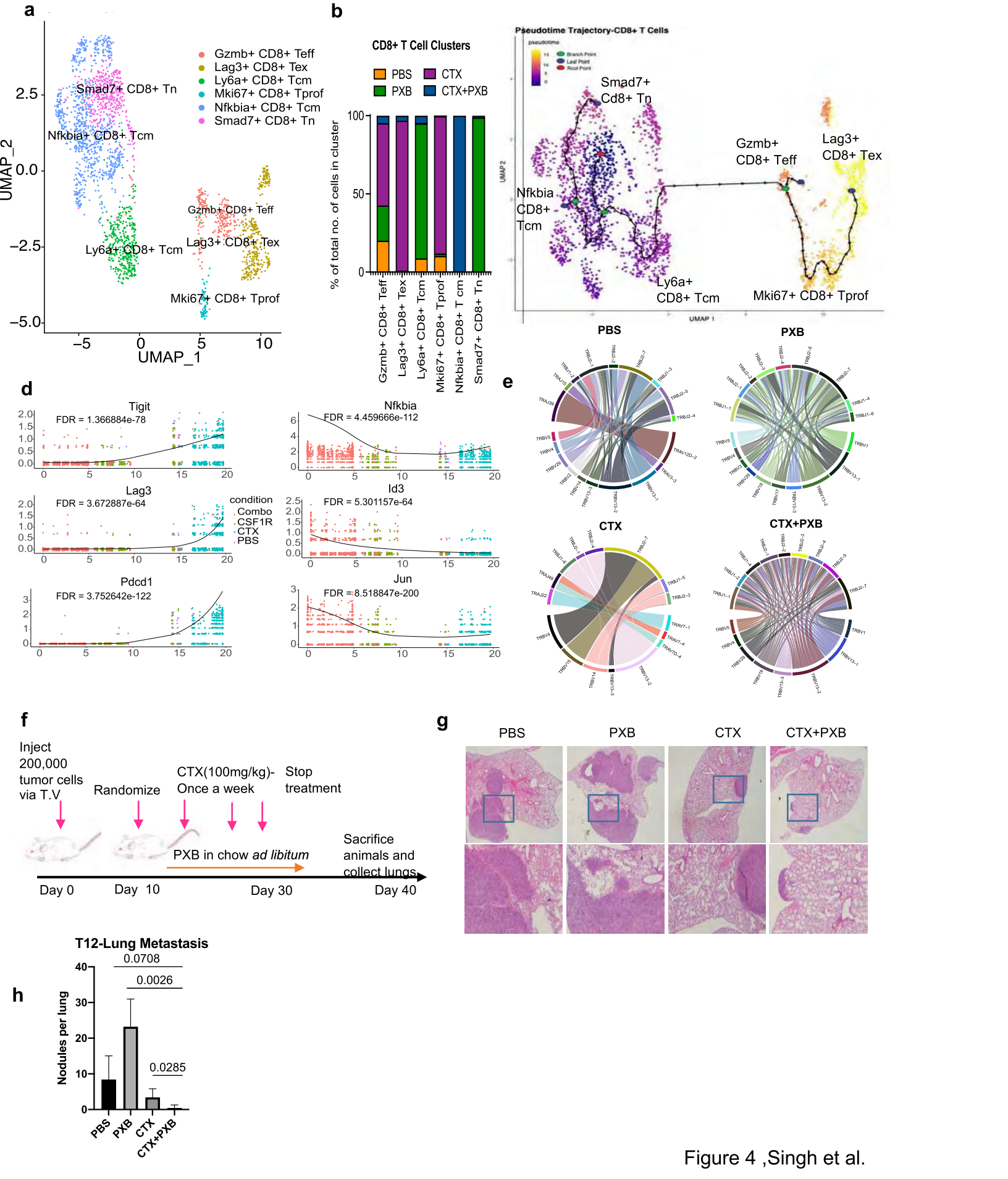

Figure 4 ,Singh et al.

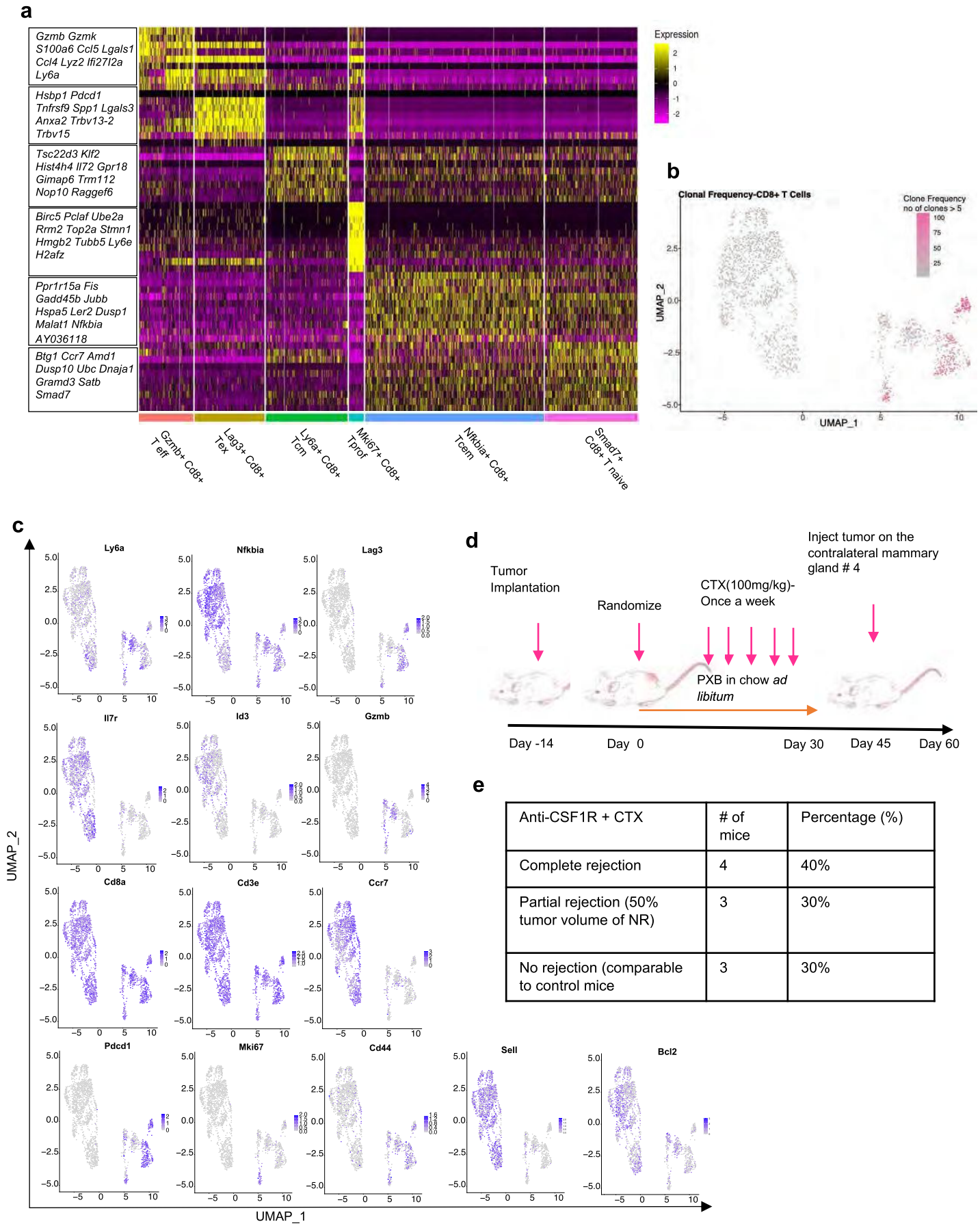

Anti-CSF1R + CTX	# of mice	Percentage (%)
Complete rejection	4	40%
Partial rejection (50% tumor volume of NR)	3	30%
No rejection (comparable to control mice	3	30%

Supplementary Figure 4 for Figure 4, Singh et al.

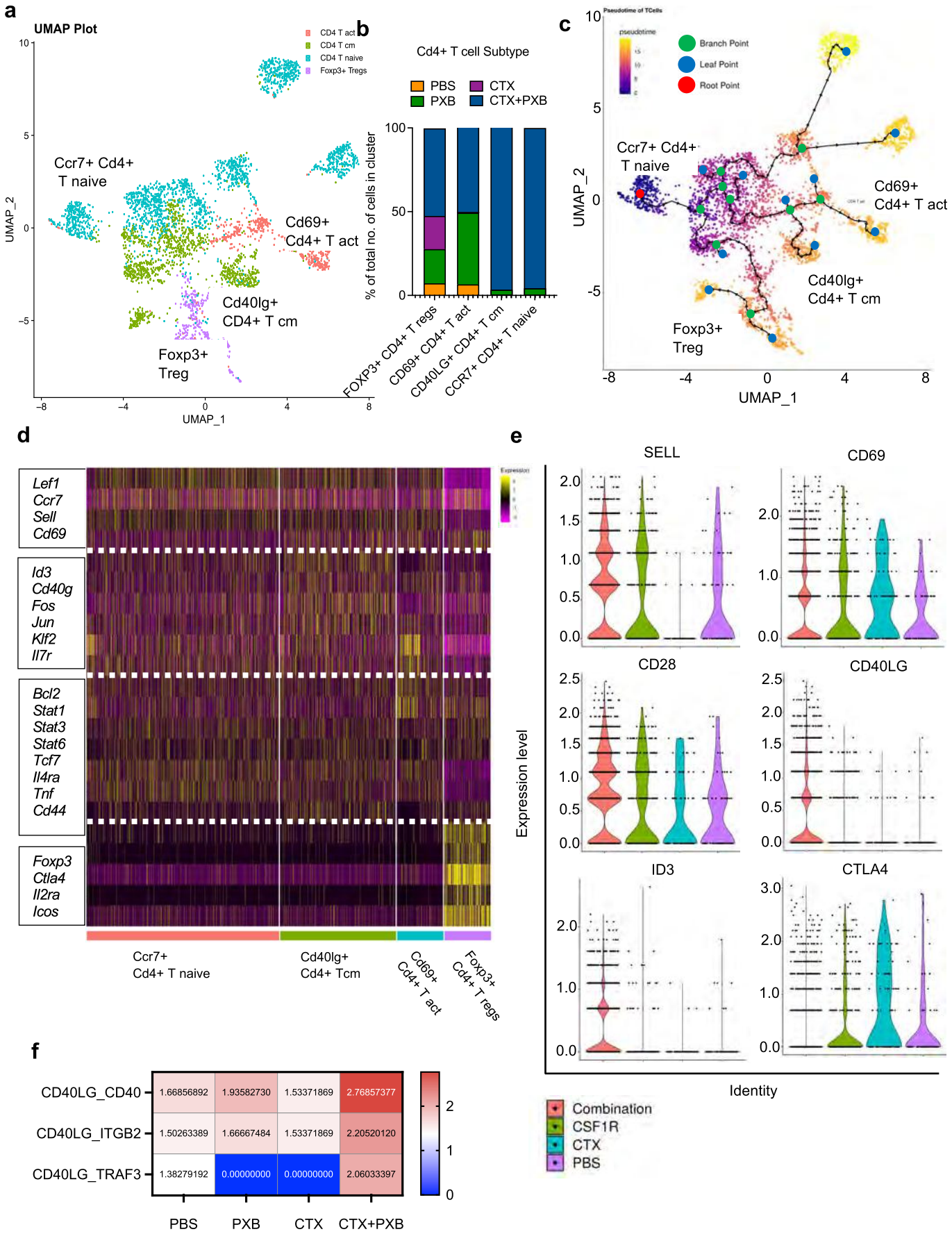

Figure 5, Singh et al.

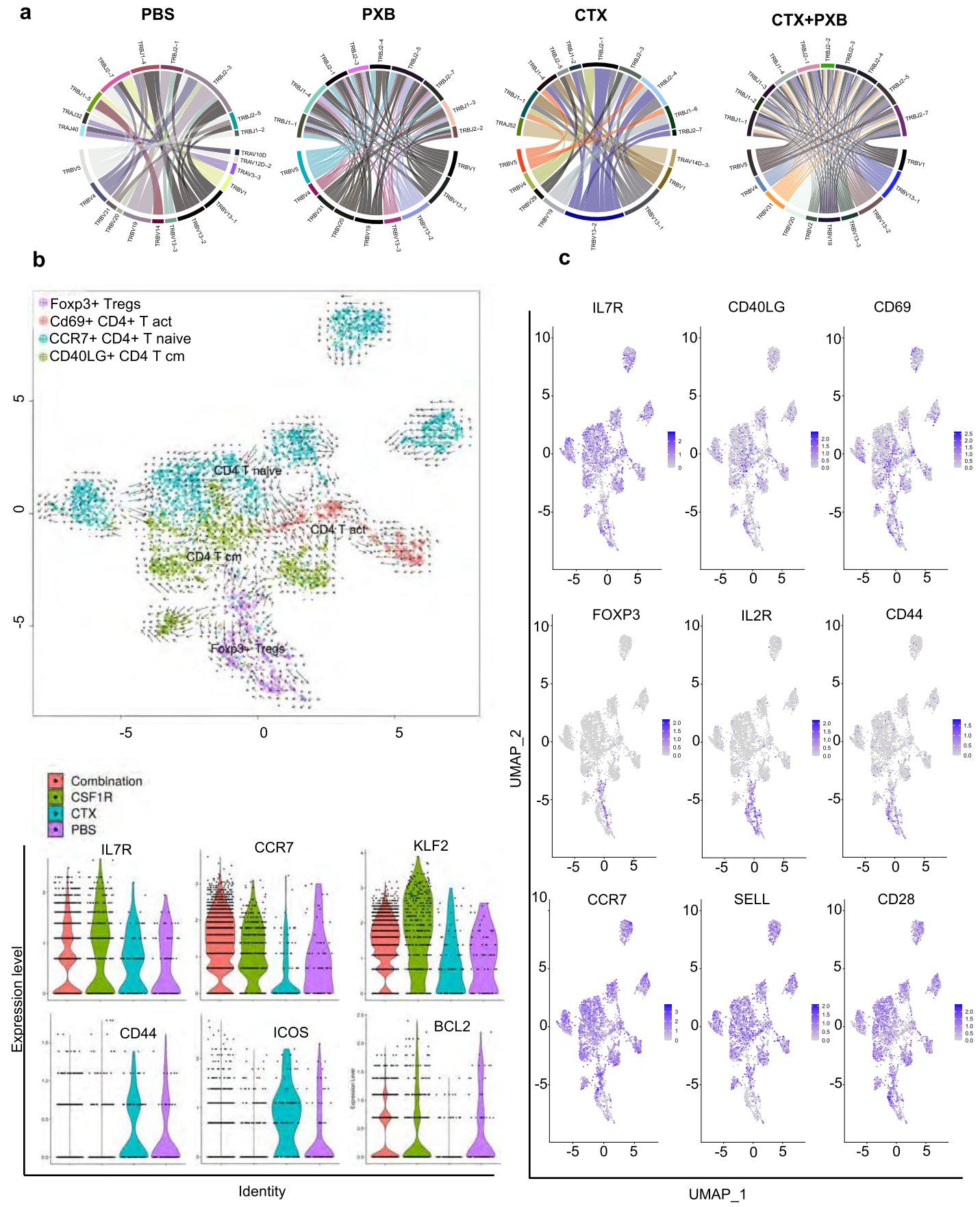

Supplementary Figure 5 for Figure 5, Singh et al.

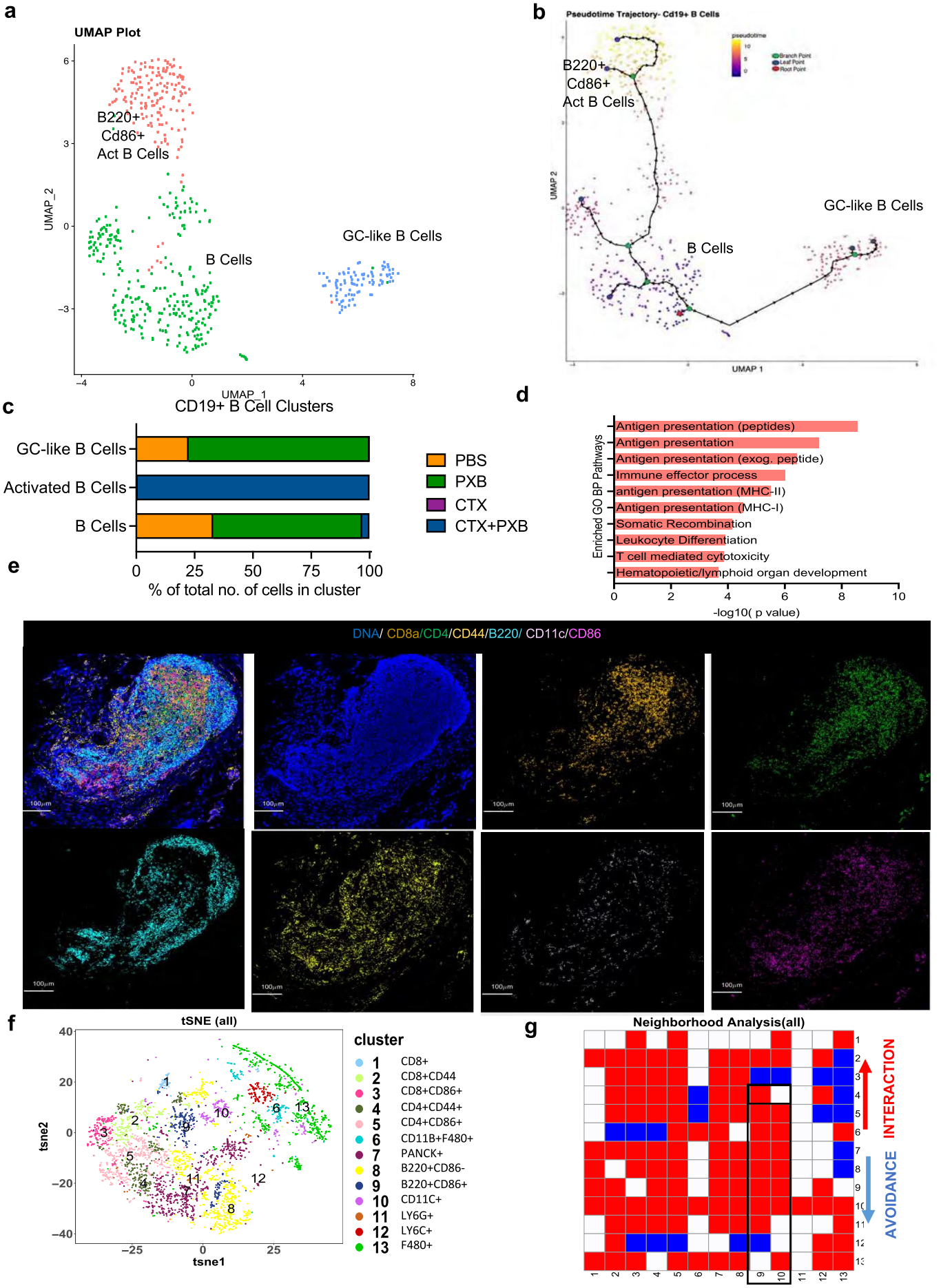

Figure 6, Singh et al.

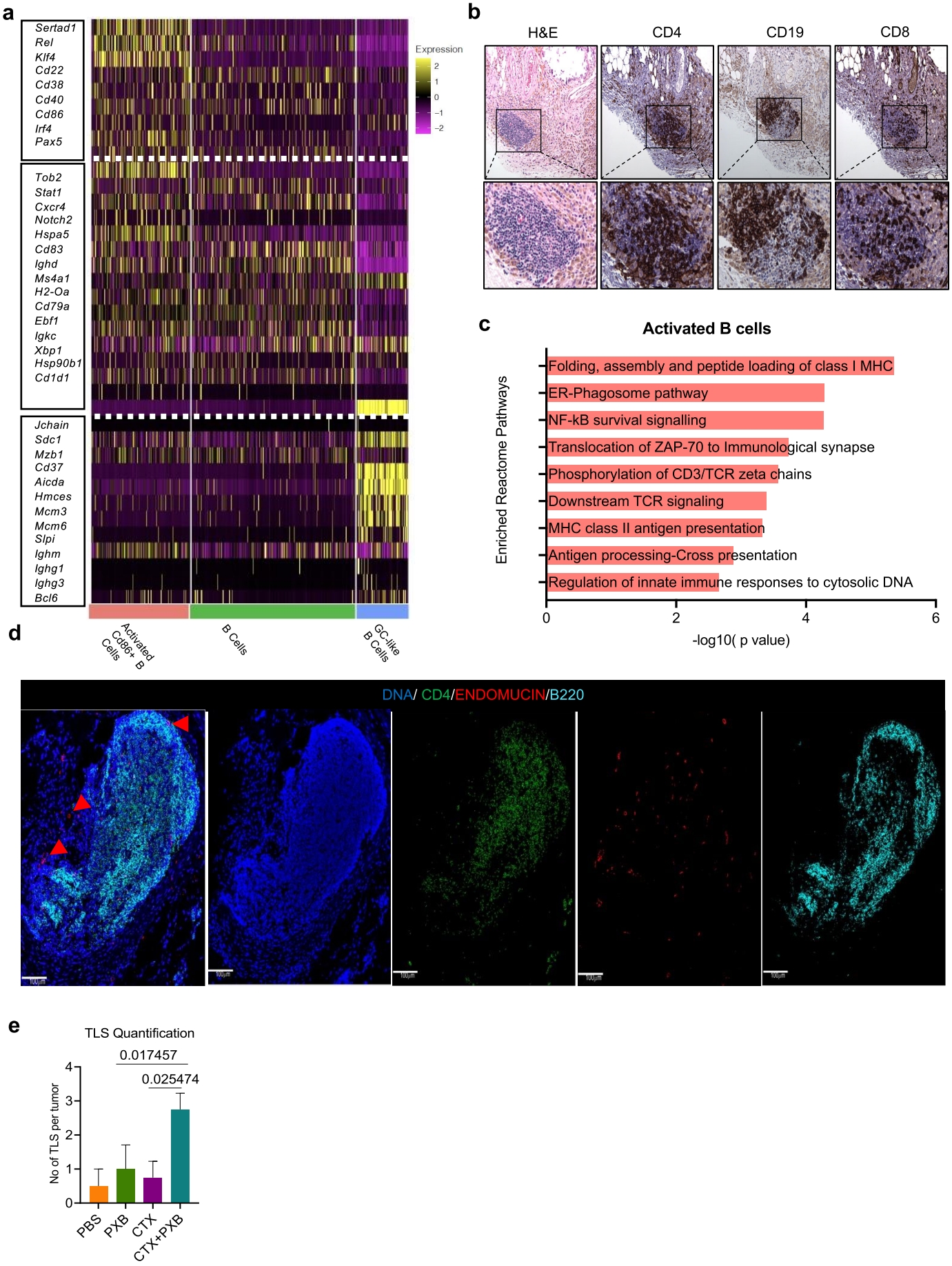

Supplementary Figure 6 for Figure 6, Singh et al.

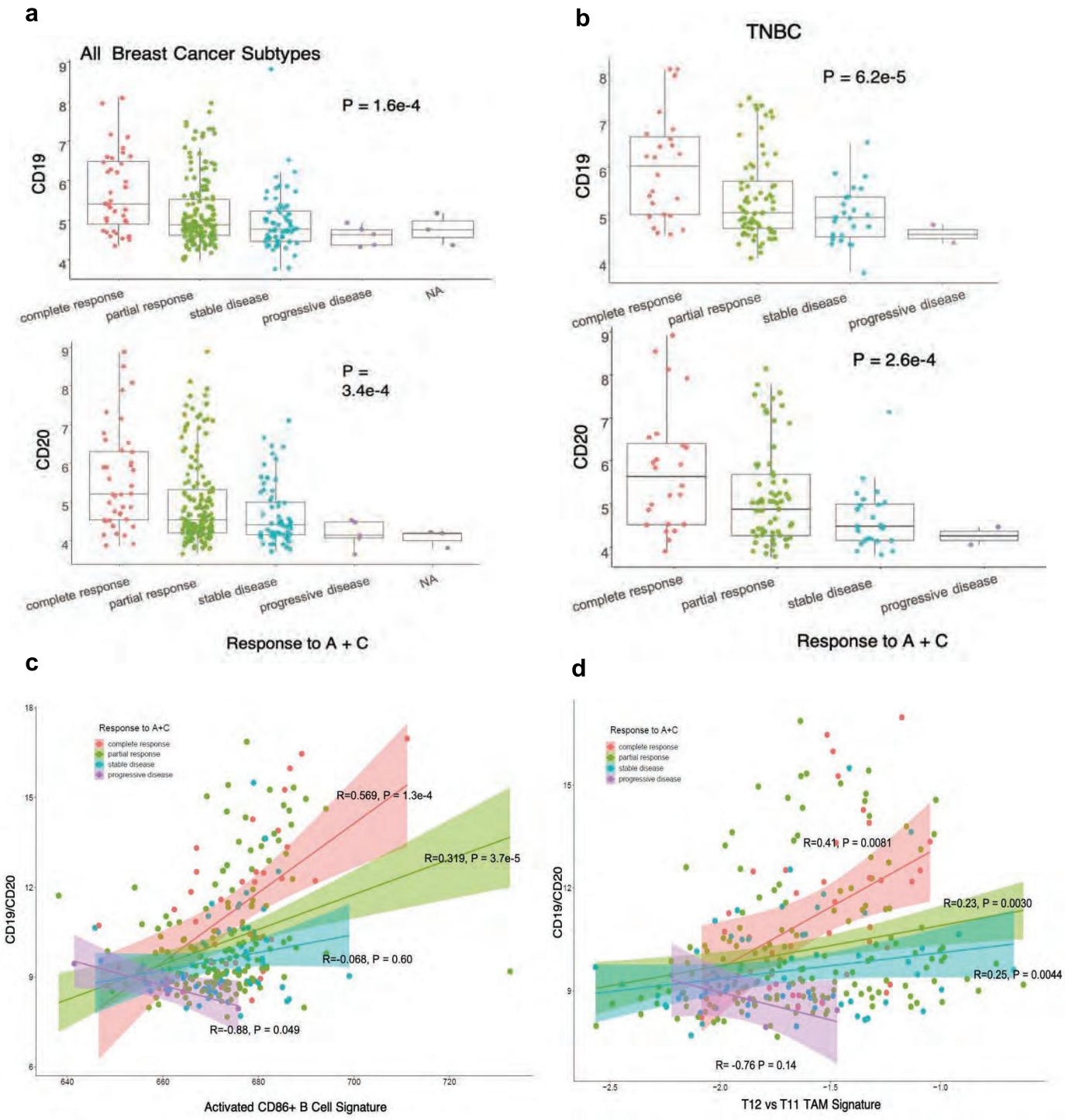

Figure 7, Singh et al.

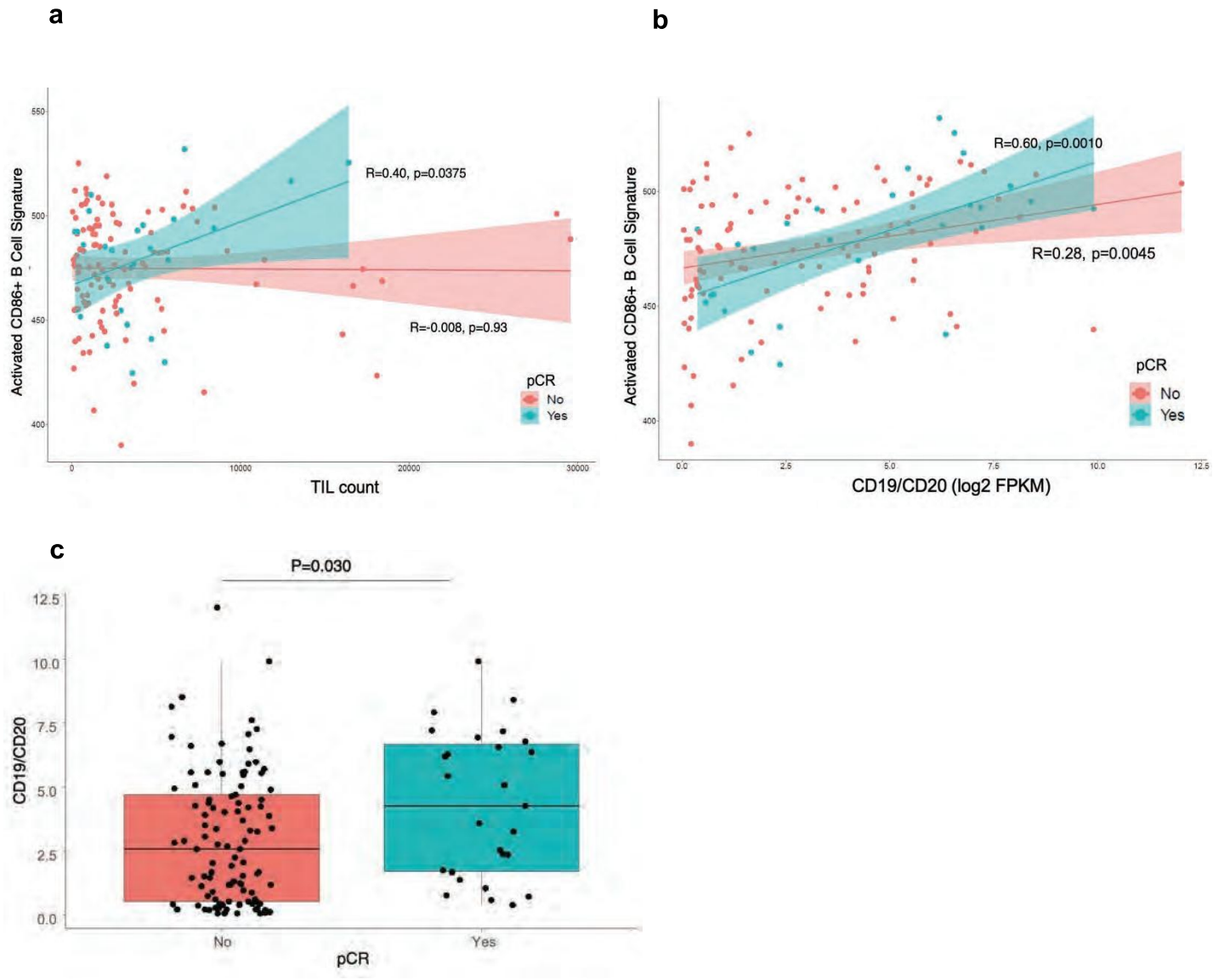

Supplementary Figure 7 for Figure 7, Singh et al.